Title Page

Title: Using *gridCoal* to assess whether standard population genetic theory holds in the presence of spatio-temporal heterogeneity in population size

Authors: Enikő Szép[1,*], Barbora Trubenová[1,2,*], Katalin Csilléry[3]

[*] Authors contributed equally

Institutional affiliations:

[1] IST Austria (Institute of Science and Technology Austria), Klosterneuburg, Austria

[2] Department of Environmental Systems Science, ETH Zurich, Zurich, Switzerland

[3] Biodiversity and Conservation Biology, Swiss Federal Research Institute WSL, Birmensdorf, Switzerland

Corresponding author:

Barbora Trubenová

Running headline: Spatio-temporal heterogeneity in population size

Acknowledgements:

ES was supported by an IST studentship provided by IST Austria. BT was funded by the European Union's Horizon 2020 research and innovation programme under the Marie Sklodowska-Curie Independent Fellowship (704172, RACE). This project received further funding awarded to KC from the Swiss National Science Foundation (SNSF CRSK-3_190288) and the Swiss Federal Research Institute WSL. We thank Nick Barton for many invaluable discussions and his comments on the thesis chapter and this manuscript. We thank Peter Ralph and Jerome Kelleher for useful discussions and Bisschop Gertjan for comments on this manuscript. We thank Fortunat Joos for providing us with the raw data from the LPX-Bern model for silver fir, and Willy Tinner for helpful insights about the demographic history of silver fir. We also thank the editor Alana Alexander for useful comments and advice on the manuscript.

Abstract

Spatially explicit population genetic models have long been developed, yet have rarely been used to test hypotheses about the spatial distribution of genetic diversity or the expected neutral levels of genetic divergence between populations. Here, we use spatially explicit coalescence simulations to explore the properties of the island model and the two-dimensional stepping stone model under a wide range of scenarios with spatio-temporal variation in deme size. We avoid the simulation of genetic data, using the fact that under the studied models, summary statistics of genetic diversity and divergence between demes can be approximated from coalescence times. We perform the simulations using *gridCoal*, a flexible spatial wrapper for the software *msprime* (Kelleher *et al.*, 2016) developed herein. In *gridCoal*, deme sizes can change arbitrarily across space and time, and migration rates between individual demes can be specified. We identify the different factors that can cause a deviation from the theoretical expectations, such as the simulation time in comparison to the effective deme size and the spatio-temporal autocorrelation across the grid. Our results highlight that F_{ST}, a measure of the strength of population structure, principally depends on recent demography, which makes it robust to temporal variation in deme size. We also warn that predicting genetic diversity from coalescence times requires a much longer run time than needed for the estimation of F_{ST}. Finally, we illustrate the use of *gridCoal* on a real-world example, the range expansion of silver fir (*Abies alba* Mill.) since the Last Glacial Maximum, using different degrees of spatio-temporal variation in deme size.

1 Introduction

The distribution and dynamics of genetic diversity within species are shaped by a myriad of evolutionary and ecological processes acting across different spatial and temporal scales

(Ellegren & Galtier, 2016). Although the role of space and, in particular, spatial autocorrelation in allele frequencies have been recognised since the dawn of population genetics (Wright, 1943; Malécot, 1948; Felsenstein, 1976; Sokal & Wartenberg, 1983), disproportionately more theoretical and methodological developments have been focused on understanding the effect of temporal changes in population size and gene flow among populations without spatial structure (*e.g.* Hey & Nielsen, 2007). Further, most statistical tools have been developed to detect past population size changes, either by testing different hypotheses such as exponential growth and bottlenecks (*e.g.* Excoffier *et al.*, 2013), or by using Bayesian methods to detect arbitrary population size changes from whole genome sequences (*e.g.* Drummond *et al.*, 2005). Researchers in landscape genetics have set the aim of overcoming the limitation imposed by population genetics methods that rely on the assumption of non-spatial and discrete populations (Manel *et al.*, 2003). However, the field has been mostly influenced by meta-population models (Hanski & Gilpin, 1991) and by spatial statistics and geo-statistics (*e.g.* Guillot *et al.*, 2005; Smouse *et al.*, 2008; Forester *et al.*, 2016), rather than by population genetic theory.

There is increasing evidence that ignoring space can lead to biases and erroneous inferences (Bradburd & Ralph, 2019). Indeed, simulation studies have shown that ignoring isolation by distance can lead to false positives in efforts to detect hierarchical population structure and loci under selection (Meirmans, 2012). Similarly, ignoring space can severely bias common population genetics summary statistics, especially when the local effective population size (i.e. neighbourhood size) is small (Battey *et al.*, 2020). However, spatially explicit models are often mathematically intractable and theoretical predictions are valid only under limited conditions (Slatkin, 1985; Barton *et al.*, 2002; Kelleher *et al.*, 2014; Bradburd & Ralph, 2019). This is particularly true for spatially continuous models. For example, the coalescence process under the continuous space isolation-by-distance (IBD) model (Wright, 1943; Malécot, 1948) can be approximated using the Lambda-Fleming-Viot algorithm (Barton *et al.*, 2010a,b). However, results are inconsistent with large-scale patterns and often predict lower diversity than expected

from census numbers (Barton *et al.*, 2010a), although some of these issues have been solved by the subsequently introduced model of extinction and recolonisation (Kelleher *et al.*, 2014). Discrete spatial models are worse at capturing reality but are mathematically more tractable (Cox *et al.*, 2002), and several equivalences have been shown across island models, two-dimensional (2D) stepping stone models (Kimura, 1953) and IBD models assuming infinite or finite populations and the absence or presence of mutations (Malécot, 1975; Felsenstein, 1976; Slatkin, 1985). In particular, a 2D stepping stone model can approximate the decrease in genetic correlation with increasing distance of continuous space (Malécot, 1955; Kimura & Weiss, 1964), and when a sufficiently large lattice is used, it can produce summary statistics similar to those from a continuous space model (Battey *et al.*, 2020).

Efficient spatially explicit simulators have recently been developed, both those using a forward in time approach, such as *SLiM* (Haller & Messer, 2019), and those using a mixture of forward and coalescent approaches, such as *SPLATCHE 3* (Currat *et al.*, 2019). These developments have increasingly enabled the inclusion of space in population genetics applications(*e.g.* Battey *et al.*, 2020; González-Serna *et al.*, 2019; Ortego & Knowles, 2020; Quilodrán *et al.*, 2019). However, these spatial simulators can be challenging to parametrise. This is particularly true for forward simulations, as they require background knowledge on the demography, mating system and dispersal patterns. Backward, coalescent simulations have the advantage of allowing likelihood calculations while only tracing back the genealogy of sampled individuals (Felsenstein, 1992). Nevertheless, they still also require that past population size changes are known or follow a predictable pattern, such as constant size, expansion, decline or bottleneck. Ecological models, such as species distribution models coupled with recently developed paleo-climatic databases (*e.g.* Lima-Ribeiro *et al.*, 2015; Cook *et al.*, 2015; Karger *et al.*, 2021), may be used to predict past species distributions in a spatially and temporally explicit manner (*e.g.* Tallavaara *et al.*, 2015; Wang *et al.*, 2017; Lima-Rezende *et al.*, 2019). Such time series of species distribution maps can provide potential input parameters for spatially explicit

coalescent simulations (He *et al.*, 2013).

The aim of this work is to explore the properties of island models and 2D stepping stone models under a wide range of scenarios with spatio-temporal variation in population size. To this end, we first develop a spatially explicit coalescent wrapper, *gridCoal*, for the most efficient coalescent simulator currently available, *msprime* (Kelleher *et al.*, 2016). In *gridCoal*, we implement the 2D stepping stone model with population sizes that may vary in space and time, and with migration rate that may differ between demes. *gridCoal* is different in several ways from *SPLATCHE 3*, the spatially explicit coalescent simulator that is currently used most frequently. Most importantly, in *gridCoal* (i) there is no forward simulation phase; (ii) demes do not follow a logistic growth model (as in *SPLATCHE 3*), instead instantly increasing or decreasing to user-defined deme sizes; and (iii) colonisation is possible from several seeds (without defining "layers" as in *SPLATCHE 3*). Further, unlike *SPLATCHE 3*, *gridCoal* does not simulate genetic marker data. Instead, we exploit the fact that under the 2D stepping stone model, summary statistics of genetic diversity and divergence between populations can be approximated from the coalescence times (Slatkin, 1991; Ralph *et al.*, 2020). After developing the coalescent wrapper, we use *gridCoal* to simulate various scenarios of spatial and temporal changes in population size and compare their outcome with theoretical expectations of the island models and 2D stepping stone models. In particular, we compare simulations with expectations for the mean coalescence time, which is proportional to the effective population size N_e and the amount of genetic diversity, for a measure of the strength of population structure F_{ST}, and for isolation-by-distance patterns. Our simulated scenarios include simplified and biologically realistic cases of population movement and expansion, where the spatial and temporal autocorrelation are decoupled. Finally, we illustrate the use of *gridCoal* on a real-world example, the range expansion of silver fir (*Abies alba* Mill.) since the Last Glacial Maximum, using different degrees of spatio-temporal variation in deme size.

2 Materials and Methods

2.1 The simulation tool: *gridCoal*

We developed a 2D stepping stone coalescent simulation tool, *gridCoal* (Appendix A), based on *msprime* (Kelleher *et al.*, 2016). Space is represented by a rectangular grid (size $L \times L$ in most of our simulations). Each grid cell contains a single panmictic population, hereafter referred to as a deme, whose size (N) can change in time at equally spaced time points comprising a given number of generations. A forward migration matrix defines the fraction of individuals that migrate from one deme to its four neighbouring demes. Forward migration rates (m) are independent from deme sizes, and they can be symmetric or asymmetric between demes, and homo- or heterogeneous across space. The backward migration matrix, required for the coalescent process, contains elements that specify the fraction of individuals in a given deme that have a parent in another deme. Backward migration rates are calculated for each time point based on the deme sizes and the forward migration matrix.

The coalescent process consists of two phases: a scattering phase in the recent past with the fully defined demographic history of individual demes, and a collecting phase in the more distant past assuming panmictic population(s). While spatial structure is important in the scattering phase, its effect becomes smaller and even negligible in the collecting phase, which can be thus approximated by the standard coalescent process (Wakeley, 1998, 1999). This implies that it is unnecessary to run the spatially explicit simulations until all lineages coalesce; before that point, the lineages can instead be combined to a single or a few spatially non-explicit panmictic populations. It is, nevertheless, possible to specify multiple ancestral populations with low migration among them, and thus account for the spatial aspect of the collecting phase.

Time is managed in *gridCoal* using three parameters: (1) the number of time points T when the deme sizes are defined, (2) the time period that elapses between two time steps dt (in years, or

other suitable time units), and (3) the generation time gt (in years or other time units, compatible with dt; see also Table 1). Thus, $T \times dt$ determines the length of the spatially explicit phase. To achieve the highest efficiency, this time should be equal to the scattering phase. After this phase, all lineages are combined into one or more panmictic, spatially non-explicit, so-called ancestral population(s). This non-spatial phase ensures that all lineages coalesce even when the product of the effective population size and migration rate (Nm) is small, and it facilitates the simulation of different refugial populations that may colonise different parts of the grid. Note that mutation is assumed to be negligible throughout this work.

2.2 Simulated scenarios

Here, we provide a brief summary of the simulated scenarios, while more details can be found in Appendix B. Across all scenarios, we used a forward migration rate that is constant in time and homogeneous across the grid. Simulations were run with an average deme size of $N \in (10, 50, 100, 250, 500)$, with migration rate $m \in (10^{-5}, 10^{-3}, 10^{-2}, 10^{-1}, 10^{0})$ between neighbouring cells (see Table 1 for explanations of terms and symbols). To analyse the effect of spatial heterogeneity, we simulated various maps differing in the amount of spatial variation and autocorrelation in deme size (Fig. 1). Our simulated scenarios ranged from a homogeneous map, where all demes have the same size, to a map with large variance in deme size, with deme sizes drawn from a uniform distribution. To investigate the effect of temporal changes, we simulated scenarios with various demographic histories: static scenarios with fixed deme sizes in time; simple demographics, where all demes changed in the same manner on average, such as undergoing an expansion, decline or bottleneck; and more biologically realistic scenarios of colonisation from one side or from "seeds" (such as refugia), or range expansion and shift (Fig. 1). For each scenario and combination of N and m in a factorial design, we ran 1000 replicates.

We sampled lineages across the grid in two different ways. In order to estimate the within-deme coalescence time, we sampled two lineages from each deme. In contrast, for

studying between-deme coalescence times, we sampled lineages along a horizontal line (L demes) in the middle of the grid.

2.3 Summary statistics

Hudson *et al.* (1990) and Slatkin (1991) noted the close relationship between the probabilities of identity by descent and coalescence times, which makes it possible to bypass the simulation of genetic data, instead estimating diversity and divergence statistics directly from coalescence times (Ralph *et al.*, 2020). Additionally, for such calculations it is sufficient to simulate the genealogies of two lineages per deme.

Coalescence times For low and high Nm, the individual demes and the grid as a whole, respectively, are nearly panmictic, the distribution of coalescence times is close to exponential, and most lineages coalesce within the scattering phase. Under these conditions, the maximum likelihood estimate of the mean coalescence time is the sample mean. In contrast, for intermediate Nm, the probability that lineages migrate away from their present-time demes before coalescing is high, but the probability that they meet again and coalesce within the spatially explicit phase of the simulation is low. As a result, the distribution of coalescent times is no longer exponential and the sample mean is an incorrect estimate of the coalescent time. In order to still consider these intermediate Nm values, we use the sample median, which is expected to be less sensitive to the missing tail values (Fig. S1).

We calculated the expected within-deme coalescence time (T_W) as the coalescence time of two lineages from the same deme. Assuming a mutation model, measures of within-population genetic diversity can be calculated from T_W. Here, we simply used T_W as a proxy for within-deme diversity and plotted it as a heatmap across the grid. T_B is the coalescence time between any two lineages from two different demes, and T_T is the coalescence time of any two lineages across the grid.

Population structure ($\mathbf{F_{ST}}$) Under the infinite island model, the extent of population structure can be described as in Whitlock & McCauley (1999):

$$F_{ST} = \frac{1}{4Nm + 1} \tag{1}$$

Under Kimura's 2D stepping stone model, given a homogeneous migration rate and equal sized demes, F_{ST} can be defined as follows (Maruyama, 1977; Cox *et al.*, 2002):

$$F_{ST} = \frac{\frac{L^2 logL}{2\pi\nu\sigma^2}}{\frac{L^2 logL}{2\pi\nu\sigma^2} + 2NL^2} \tag{2}$$

where $\sigma = 1/2$ is the average axial parent–offspring distance, $\nu = 4\mu$, and L is the grid size. The value $2\pi\nu\sigma^2$ is the neighbourhood size, which is the local panmictic unit that determines the amount of variation between populations at the migration–drift equilibrium; thus, it is equivalent to Nm in the island model. Note that when $\frac{logL}{2\pi\nu\sigma^2} << 2N$, equation (2) simplifies to $F_{ST} = \frac{logL}{4N\pi\nu\sigma^2}$ (Cox *et al.*, 2002).

The link between F_{ST} and coalescent theory was introduced by Slatkin (1991):

$$F_{ST} = \frac{T_T - T_W}{T_T} \tag{3}$$

where T_T is the average total coalescence time and T_W is the within-deme coalescence time averaged across demes. We refer to equation (3) as the *global* (population-wide) F_{ST}, which measures the strength of the population structure and can be compared across different simulated scenarios, and we use this definition throughout the manuscript. Note that approximating summary statistics of genetic diversity and F_{ST} from coalescence times holds only when the mutation rate is low, and migration is possible to neighbouring demes only (Slatkin, 1985).

Genetic distance (F^*) In order to investigate the genetic differentiation between pairs of demes and its relationship with physical distance, we used a measure of genetic distance based on coalescence times. If only two demes are considered, Equation 3 transforms into:

$$F^* = \frac{T_B - T_W}{T_B + T_W} \tag{4}$$

where T_B is the mean coalescence time for two lineages sampled from different demes, and T_W is the mean within-deme coalescence time. Slatkin (1993) pointed out that this equation is not appropriate to asses the strength of population structure in general, but it is a useful measure of the genetic distances between demes. We used F^* between all pairs of sampled demes against the physical (Euclidean) distance between demes to assess isolation-by-distance patterns across the grid. Note that if $T_W \approx T_B$ (which is the case for large Nm), $F^* = \frac{F_{ST}}{2-F_{ST}}$ and F^* thus does not provide any more information about the population structure than F_{ST}.

Effective population size (N_e) Under the island model, N_e is

$$N_e = Ns\left(1 + \frac{(s-1)^2}{4N\nu s^2}\right), \tag{5}$$

where $\nu = 4m$ (the total migration rate for each grid cell), and s is the number of demes in the island model. While, N_e under two dimensional stepping stone model can be calculated as Cox *et al.* (2002):

$$N_e = \frac{L^2 \log(L)}{4\pi\sigma^2\nu} \tag{6}$$

Effective population sizes predicted from simulations were obtained by halving the coalescence time of lineages from the same deme.

3 Results

3.1 Coalescence times

The expected coalescence time of two samples drawn from the same deme is $T_W = 2N$, where N is the total number of diploid individuals in the deme. This result is independent of the migration matrix if all demes are connected by migration. Under the island model with d demes each containing N individuals, the expected coalescence time for two samples from the same deme is $2Nd$ (Strobeck, 1987), which is higher then $2N$ as a result of lineages escaping before coalescence occurs. Under the 2D stepping stone model the expected coalescence time is $2NL^2$ (Cox *et al.*, 2002). However, in a 2D stepping stone model, where only the four neighbours are connected, strong local differentiation across demes occurs when $Nm < 1$ (Kimura & Maruyama, 1971). In contrast, when $Nm > 1$ local differentiation is less pronounced, and when $Nm \geq 4$ the whole grid behaves like a single panmictic population (Kimura & Maruyama, 1971). Our simulations helped us to explore the effect of spatial heterogeneity in deme size on these theoretical predictions.

Spatial heterogeneity can be ignored when $m = 0$ and thus each individual deme behaves like a panmictic population. In these cases, the expected coalescence time for two samples taken from the same deme is independent of the spatial heterogeneity of the grid and is thus expected to be $2N$ (Fig. 2a and d). However, for the largest deme size considered ($N = 500$), T_W was on average larger than $2N$. At the other extreme, when m was one, the whole grid behaved like a single panmictic population. Here, T_W was decoupled from the local deme size and was, on average, equal to $2NL^2$ (Fig. 2c). Additionally, when there was large spatial variance in deme size across the grid, the uniform map, the coalescence time was systematically underestimated (Fig. 2f). This was because the spatial heterogeneity decreased the total effective population size across the grid.

For low migration rates, the expected coalescence time of two samples from the same deme

should be $T_W = 2NL^2$, independent of m (Maruyama, 1971). When m is very small, lineages coalesce mostly within demes, on average, in time $2N$. However, very rarely, they escape and coalesce only in time $2NL^2/m$, which results in a mean coalescence time of $T_W = 2NL^2$. The spatially explicit phase of our simulations was not long enough for these samples to coalesce after they escaped from the deme, and these were thus forced to coalesce sooner, leading to underestimation of the average coalescence time (Fig. 2b and e). The problem of escaping lineages matters the most in the transition phase from low to high Nm. Recall that in this part of the parameter space we could not estimate the sample mean; therefore, we show the median T_W instead (Fig. 2). Note that these results should be treated with caution and cannot be compared with any theoretical expectations. We found that for $Nm \leq 0.05$, T_W was best predicted by $2\bar{N}$ (Fig. 2b; $m = 0.001$ and $N = 50$). Then, for $Nm = 0.1$, our simulations showed that the median coalescence time was best predicted by twice the neighbourhood size, i.e. the size of the deme plus its four neighbours (Fig. 2e; $m = 0.001$ and $N = 100$). However, we found that already at $Nm = 0.5$ the coalescence time was best predicted by $2NL^2$ (Fig. 2; see also Fig. S1b and e), suggesting that the transition phase is fast, which is in agreement with previous observations by Kimura & Maruyama (1971) .

3.2 Global F_{ST}

The island model (eq. 1) and 2D stepping stone model (eq. 2) provide expectations for the strength of population structure (F_{ST}) in subdivided populations. Here, we explored the robustness of these predictions with respect to the spatio-temporal heterogeneity in deme size. We found that all simulated scenarios deviated the most from theoretical predictions for intermediate migration rates (or Nm), where the predictions of the two models also differed the most (Fig. 3a, b and c). Not surprisingly, the island model provided, on average, a better approximation than the spatially explicit 2D stepping stone model when the deme sizes were drawn from a uniform distribution across the grid, thus when there was no spatial

autocorrelation in deme size (Fig. 3a). In contrast, when deme sizes were homogeneous across space, and thus the spatial autocorrelation was maximised, F_{ST} was closer to the 2D stepping stone model predictions (Fig. 3a). F_{ST} of the clustered and low variance maps were in between the two model predictions. F_{ST} also varied considerably across replicates, with the largest variation occurring for the uniform map among all static scenarios considered (Fig. 3d).

Across the changing scenarios, we observed a consistent bias: scenarios where the mean deme size decreased over time gave a lower F_{ST}, while scenarios where the mean deme size increased (expanding population) gave a higher F_{ST} in comparison to the static equivalent scenarios (Fig. 3b and c). Similar to with the uniform static map, F_{ST} was relatively close to the predictions of the island model under the changing scenarios that ended in a uniform map (Fig. 3b). More unexpectedly, under the realistic changing scenarios, where we decoupled the spatial and temporal autocorrelation, on average, F_{ST} did not deviate more from the island model prediction than the simple changing scenarios for the studied parameter combinations (Fig. 3c). These realistic changing scenarios also provided a relatively close match to their static equivalents (Fig. 3c). An exception is the range expansion and shift scenario. This is because here the theoretical expectation is shown for the average N across the grid, which is lower than the row of sampled demes situated in the middle of the grid (Fig. 1). Finally, the variation in F_{ST} across replicates was important, and F_{ST} for different realisations of the same map overlapped between values of Nm that were one order of magnitude different, especially for low and intermediate values (Fig. 3d, e and f). The sampling variance in F_{ST} also increased with spatial variance in deme size across the grid, with the highest values corresponding to the two clustered maps (Fig. 3d and f).

3.3 Genetic distance (F^*)

Varying N and m across a homogeneous map showed that increasing the deme size and/or the migration rate led, as expected from equation (1), to weaker differentiation between demes (Fig.

S2). The degree of spatial variance in deme size affected both the average genetic distance between demes and the shape of the isolation by distance curves (Fig. 3g). Maps with homogeneous deme size had the lowest and flattest isolation by distance curves. Note that these can be treated as a baseline expectation under the 2D stepping stone model (Slatkin, 1993). The uniform map gave higher F^* values across all the distance classes, i.e. the isolation by distance curve was shifted upwards, because the compared pairs of demes had, on average, a different size. The clustered map resulted in a lower mean F^* for small distance classes and a higher F^* for larger distance classes, meaning that the isolation by distance curve was steeper. This was because pairs of demes located close to each other tended to have similar sizes, and those for large distance classes often had different sizes. Varying deme classes also caused a large variance in the genetic distance across replicates (Fig. 3g, h and i).

Demographic, i.e. temporal, changes introduced a bias in the same direction as in F_{ST}: scenarios where the mean deme size decreased over time had a lower F^*, while scenarios with increasing average deme size had a larger F^* value in comparison to a static uniform map. However, the shape of the isolation by distance curve did not change (Fig. 3h). The realistic changing scenarios all had increasing deme sizes, so we observed the same upward bias as before (Fig. 3i). The fact that the population sizes were changing had the strongest influence on F^* when the spatial and temporal autocorrelation was the most decoupled, i.e. for the side colonisation scenario, and for large distance classes (Fig. 3i).

3.4 Effect of spatial and temporal resolution

Our simulations were carried out on a finite square grid of $L \times L$ (not a torus), which implies a finite number of demes and that demes on the edge of the grid had only two or three neighbours. Not surprisingly, we found that F_{ST} estimated from a larger grid provided a better fit to the predictions of the island model and the 2D stepping stone model (Fig. 4a). Further, we found that there was an edge effect, which led to the overestimation of F^* for demes that were L or nearly L

steps away from each other (Fig. 4b). Analysing F^* against distance from samples in the middle the grid allowed us to disentangle the effect of grid size from the edge effect. We found that close to the edges the genetic distance is overestimated between the demes, mainly due to edge effects, while grid size principally influences the precision of the estimates, i.e. larger grids provide more precise estimates of F^* for a given distance class (Fig. 4c).

We investigated the effect of temporal resolution in the case of a simple changing scenario where all demes increased linearly in size (Fig. 1). The coarser time resolution ($T = 5$) did not have a noticeable effect on the estimation of the mean coalescence time within demes, but the between-deme coalescence times were systematically overestimated (not shown). As a result, the genetic distances between demes were also overestimated (Fig. 4e). This is because when $T = 5$, the population size at any time is larger than in the finer time-resolution scenario ($T = 25$). Time resolution is also important in more complex setting such as range expansion and shift (Fig. 1).

The time necessary for lineages to coalesce during the spatially explicit phase of the simulations may become a limitation in practical applications. When the spatially explicit phase is too short compared with the deme sizes, the coalescence time between lineages is determined by the non-spatial coalescence process of the panmictic ancestral population. Extremely long simulations may be required to reliably estimate the coalescence time when the deme sizes are large. Fig. 4e shows estimates of N_e calculated as half of the mean total coalescence time. In contrast, Fig. 4f demonstrates that it is possible to obtain relatively precise estimates of F_{ST} with much shorter simulation times. This is because F_{ST} is defined as a ratio of coalescence times and the biases cancel out. Indeed, both the estimation of within-deme and total coalescence times are biased because of the same process, i.e. the limited length of the spatially explicit phase, which means that their distributions are missing the same amount from the tails on the right side. This result also highlights that F_{ST} is dependent only on recent demographic events and is independent of the deeper ancestry, which makes it a useful measure.

3.5 Application example: *Abies alba* post-glacial colonisation history

Silver fir (*Abies alba* Mill.) is a coniferous tree species that has progressively colonised the mountainous regions of Europe from different refugia since the Last Glacial Maximum (LGM, 21 kyrs BP). While the exact location of the refugia are debated, it is generally agreed that the Central and/or Northern Apennines hosted the largest populations in pre-LGM times, with other important populations occurring on the Balkan Peninsula (Tinner *et al.*, 2013). Mitochondrial DNA variation clearly suggests the presence of two haplotypes corresponding to the Italian and Balkan Peninsulas (Ziegenhagen *et al.*, 2005; Liepelt *et al.*, 2009) (Fig. S3).

The demographic history of silver fir over the past 22 kyrs BP was obtained from the LPX-Bern dynamic global vegetation model with a resolution of 1° by 1° Lat/Lon (Sitch *et al.*, 2003; Ruosch *et al.*, 2016). The model was forced with climate anomalies and included competition between common tree species and plant functional types. The output of LPX-Bern is the Foliar Projective Cover (FPC), which is the fraction of a grid cell that is covered by silver fir. We estimated the number of trees (N) in each deme from FPC, assuming that a mature tree occupies $40\ \mathrm{m}^2$, and that $N/N_e = 0.001$ (an arbitrary but realistic value (Waples *et al.*, 2011)). The full input data consisted 221 time points spaced at 100 year (i.e. four generation) intervals on a 53×24 grid. In the following we shall refer to one grid cell of LPX-Bern as one deme. While the population size of the whole species (i.e. all demes) showed an overall increasing trend with time (post-LGM colonisation), the size fluctuations of individual demes were highly variable (see Fig. 5a). We used the expected coalescence time for two samples taken from the same deme as an approximation for the genetic diversity in a deme, thus assumed that mutations can be neglected. Finally, we note that LPX-Bern has several shortcomings and does not predict the current distribution of silver fir accurately. However, the objective of this example was not to make predictions for the expected levels of genetic diversity in silver fir, but to study the effect of spatio-temporal heterogeneity in population size in a biologically realistic scenario.

We performed four simulated scenarios. First, we used a homogeneous deme size (i.e. N_e) in space and time, which represented our null model. We fixed the deme size to its average size based on the last step of the LPX-Bern data. Second, we included the spatial variation in deme size, represented by the last step of the LPX-Bern data, but kept deme sizes constant in time. Third, we used the full LPX-Bern input data, thus considering realistic deme sizes changing both in space and in time. Fourth, we explored the effect of having two ancestral populations, i.e. using pre-LGM historical information. For this, we used simulations identical to the third scenario, but at the oldest time point (i.e. 22 kyrs BP), and we combined the demes into one of the two most plausible ancestral populations based on the spatial distribution of mtDNA haplotypes in contemporary samples (Fig. **??**a). We achieved this by simply assigning each deme with mtDNA data to the dominant haplotype (i.e. more than 50% Balkan or Italian type) or to the origin of the nearest deme of known origin, in case of missing data (Fig. **??**b).

We found that both space and time had an effect on the coalescence times, and thus on the distribution of genetic diversity in space (Fig. 5b). As expected, when the deme size was constant in space and time, the distribution of genetic diversity only reflected stochastic effects of the coalescence process (Fig. 5b, Scenario 1). Spatial variation in deme size introduced variation in the expected levels of genetic diversity, which was also proportional to the deme size (Fig. 5a and b, Scenario 2). When deme size varied both in space and time, the spatial variation in the mean coalescence time became even stronger. In particular, the recently colonised areas of Northern Europe had a lower expected level of genetic diversity (Fig. 5b, Scenario 3). Finally, when we assumed two ancestral populations, their contact zone had much higher levels of expected genetic diversity (Fig. 5b, Scenario 4). This is because there was a much longer waiting time for the two ancestral populations to coalesce, which is determined by the size of these populations and also by the migration rate between them. For a real data application, calibration of these two parameters would be necessary to match the observed genetic diversity data. Alternatively, the match between simulated and observed data could be used to estimate the divergence time

between the two mtDNA haplotypes (*e.g.* Hickerson *et al.*, 2007).

4 Discussion

The role of spatial and temporal autocorrelation

Using a wide range of simplified and biologically realistic simulations, we have identified several factors that may cause a deviation from theoretical expectations of the island model and the 2D stepping stone model. We found that non-spatial null models, such as the island model, are inappropriate in the presence of spatial autocorrelation in deme size (Fig. 3). Most real-life situations involve some degree of spatial autocorrelation. Previous studies have already demonstrated the limitations of non-spatial null models, for example in the presence of isolation by distance (Wang & Whitlock, 2003; Meirmans, 2012), due to population structure or biased sampling schemes (Chikhi *et al.*, 2010), or to local variation in deme size or barriers to gene flow across the landscape (Duforet-Frebourg & Blum, 2014). Here, we show that the 2D stepping stone model can account for spatial autocorrelation, at least when it is homogeneous across the landscape, and to some extent when there is local variation in deme size (clustered scenario) (Fig. 3). Thus far, the 2D stepping stone model has rarely been used as a null model (but see Duforet-Frebourg & Blum 2014 and Battey *et al.* 2020), partly due to the lack of a simulation tool. *gridCoal* could facilitate more widespread use of the 2D stepping stone model to generate the null distributions of neutral statistics, such as genetic diversity (assuming a non-zero mutation rate) or F_{ST}, in the presence of spatial autocorrelation in population size.

Demography, or temporal change in population size, is well known to contribute to deviations from theoretical expectations of the island model, and can limit the validity of statistical procedures that are based on this model. This is particularly true for F_{ST}-outlier tests used to detect loci under selection (*e.g.* Chikhi *et al.*, 2010; Bierne *et al.*, 2013; De Mita *et al.*, 2013; Lotterhos & Whitlock, 2014) because F_{ST} is dependent on recent ancestry (Slatkin, 1991). Here, we simulated realistic scenarios with the presence of both spatial and temporal heterogeneity in

deme size, and observed that deviations from the theoretical expectations are strongest when the spatial and temporal autocorrelation in deme size are decoupled (Fig. 3c, range expansion and shift). Our simulations demonstrate that neutral F_{ST} is well below the theoretical expectations for such a range expansion and shift (Fig. 3c). This result is in agreement with the findings of Lotterhos & Whitlock (2014), who showed that spatial autocorrelation in deme size or recent range expansion resulted in the largest number of false positives for most methods in efforts to detect spatially divergent selection. Spatio-temporal trends in population size are expected to be common in nature, especially in the Northern hemisphere, where the demographic history is often dominated by expansion from glacial refugia and a shift towards the north (*e.g.* Excoffier *et al.*, 2009). Our example application also illustrates such a case (Fig. 5).

F_{ST} and F^* are based on the same information, but F_{ST} is a more integrative and therefore more robust measure, while F^* is more sensitive to local differentiation patterns (Fig. 3g–i). Note that our F^* is closely related to $\hat{M}$ of Slatkin (1993), which has the advantage of being independent of the mutation rates when they are small across loci. Based on a wide range of scenarios, we found that spatial and temporal variation in deme size can influence the steepness of the isolation-by-distance curve. In agreement with Duforet-Frebourg & Blum (2014), we found that local variation in population size, as in our clustered map, caused large variance in local F^* (Fig. 3g). The most complex range expansion and shift scenario led to a relatively flat isolation-by-distance curve (Fig. 3i). Indeed, Slatkin (1993) already proposed that the lack of an isolation-by-distance pattern in a natural population can indicate non-equilibrium populations or recent colonisation, a pattern that has been confirmed through empirical studies (*e.g.* Leblois *et al.*, 2000; De Kort *et al.*, 2014).

gridCoal: Guidelines for future users

gridCoal is a wrapper for the most efficient algorithm to simulate genealogies: the optimised continuous time approximation of the coalescence process implemented in *msprime* (Kelleher *et al.*, 2016). It complements the existing arsenal of spatially explicit simulators (Guillaume &

Rougemont, 2006; Landguth & Cushman, 2010; Haller & Messer, 2019; Currat *et al.*, 2019; Dellicour *et al.*, 2014; Becheler *et al.*, 2019). The choice of parameters and model calibration are essential for running spatially coalescent simulations. Here we provide some guidelines in the case of *gridCoal*.

The spatially explicit phase (given by the number of steps T and the time step dt) should be long enough so that lineages coalesce during this phase, but also short enough to avoid wasting computational time. The choice of dt should be driven by the particular biological question. For example, throughout this paper we used a combination of parameter values (number of steps T, time step dt and generation time gt) such that most lineages coalesced in the spatially explicit phase across all combinations of N and m (Fig. 4d–f). Note that the largest dt was necessary for intermediate values of Nm, where lineages can escape and take a long time to coalesce. We suggest that users perform test simulations with the required values of N and m to choose an appropriate dt. This is particularly important if it is necessary that all lineages coalesce during the spatially explicit phase, e.g. for estimating genetic diversity maps such as those shown in the example of post-glacial colonisation of silver fir (Fig. 5). In contrast, if the question concerns a particular organism with a given generation time and across a particular time period, the parameters can be chosen accordingly. For example, setting $dt = 100$ and using 210 time points takes the ancestral population back to the Last Glacial Maximum (LGM, 21 kya), which could be a suitable parameter combination for several species that expanded after the LGM.

gridCoal avoids the simulation of genetic data and instead simulates summary statistics that can be derived from coalescence times, i.e. gene diversity, the strength of population structure (F_{ST}), and the genetic distance between pairs of demes (F^*). We emphasise that approximating summary statistics of genetic diversity and F_{ST} from coalescence times holds only when the mutation rate is low and when migration is possible to neighbouring demes only (Slatkin, 1985). Further, for comparing *gridCoal* simulations to real data, a calibration of N_e and μ is necessary because these parameters are non-identifiable. Such a calibration can be achieved by using additional information about the mutation rate of particular genetic markers used and by

estimating N/N_e (Waples *et al.*, 2011). Finally, simulations from *gridCoal* are closer to that of a continuous space model, and thus to biological reality, for large grid sizes. Nevertheless, at least for small neighbourhood sizes, a grid of 50×50 already appears to be sufficient to accurately approximate a continuous space process for many commonly used summary statistics (see details in Battey *et al.* 2020).

gridCoal for eco-evolutionary data fusion

gridCoal might be useful for empirical applications of eco-evolutionary data-fusion approaches, such as integrative Distributional Demographic Coalescent (iDDC) approach (He *et al.*, 2013; Brown & Knowles, 2012). In this context, one key feature of *gridCoal* is that it is not only spatially but also temporally explicit. Temporal explicitness means that the exact population size of each deme has to be set by the user at regularly placed time intervals. In this way, *gridCoal* is fully deterministic in terms of the forward-time demography, and stochastic in terms of the backward coalescence events. Although this feature may appear as a limitation in some situations, it is necessary for applications that make use of species distribution data issued from ecological models and paleological data (Svenning *et al.*, 2011; Gavin *et al.*, 2014). This feature also represents an important contrast to *SPLATCHE 3* (Currat *et al.*, 2019), where each deme follows a logistic growth model. As a result, in *SPLATCHE 3*, user-provided population sizes are only approximately achieved, no population declines, and only local extinctions are possible. Indeed, to set up explicit temporal changes in population size, Ortego & Knowles (2020) updated the population sizes only three times from 21 ky BP to the present, which is a rough approximation of actual population size changes and may bias the isolation-by-distance patterns (Fig. 4d).

There is a wide range of possible input data sets that can be used for eco-evolutionary data-fusion approaches. First, paleo-climatic databases have opened possibilities for running species distribution models (SDMs; Elith & Leathwick 2009; Sexton *et al.* 2009) and for producing a time

series of species distribution maps. Second, process-based dynamic vegetation models (DVMs; Pereira *et al.* 2010) offer important advantages over SDMs, which are static, correlative approaches, and thus DVMs hold a great potential for use in data-fusion approaches. Even though DVMs suffer from limitations related to their complex parametrisation, they are continually improving as the quality and richness of climatic, remote sensing, and other biological data increases (*e.g.* Hartig *et al.*, 2012). Third, fossil data is increasingly being organised in databases (Davis *et al.*, 2013; Peters *et al.*, 2019). The most abundant type of fossil data is pollen, particularly from forest trees, which has been used to reconstruct past population size fluctuations (*e.g.* Ruosch *et al.*, 2016; Kaufman *et al.*, 2020). Indeed, our example of post-glacial colonisation history in silver fir (see Fig. 5) could be made more realistic by using the spatio-temporal interpolation of pollen records (Ruosch *et al.*, 2016).

Data accessibility

Detailed information about the software, a user manual, and example simulations are available for download at `https://github.com/Trubenova/gridCoal`.

Author contributions

KC designed the research. ES and BT developed *gridCoal*, ran the simulations and analysed the data. ES, BT and KC wrote the manuscript.

Literature Cited

Barton N, Etheridge A, Véber A, *et al.* (2010a) A new model for evolution in a spatial continuum. *Electronic Journal of Probability*, **15**, 162–216.

Barton NH, Depaulis F, Etheridge AM (2002) Neutral evolution in spatially continuous populations. *Theoretical Population Biology*, **61**, 31–48.

Barton NH, Kelleher J, Etheridge AM (2010b) A new model for extinction and recolonization in two dimensions: quantifying phylogeography. *Evolution*, **64**, 2701–2715.

Battey C, Ralph PL, Kern AD (2020) Space is the place: Effects of continuous spatial structure on analysis of population genetic data. *Genetics*, **215**, 193–214.

Becheler A, Coron C, Dupas S (2019) The Quetzal Coalescence template library: A C++ programmers resource for integrating distributional, demographic and coalescent models. *Molecular ecology resources*, **19**, 788–793.

Bierne N, Roze D, Welch JJ (2013) Pervasive selection or is it ...? why are F ST outliers sometimes so frequent ? *Molecular Ecology*, **33**, 2061–2064.

Bradburd GS, Ralph PL (2019) Spatial population genetics: It's about time. *Annual Review of Ecology, Evolution, and Systematics*, **50**, 427–449.

Brown JL, Knowles LL (2012) Spatially explicit models of dynamic histories: examination of the genetic consequences of Pleistocene glaciation and recent climate change on the American Pika. *Molecular Ecology*, **21**, 3757–3775.

Chikhi L, Sousa VC, Luisi P, Goossens B, Beaumont MA (2010) The confounding effects of population structure, genetic diversity and the sampling scheme on the detection and quantification of population size changes. *Genetics*, **186**, 983–995.

Cook ER, Seager R, Kushnir Y, *et al.* (2015) Old world megadroughts and pluvials during the common era. *Science advances*, **1**, e1500561.

Cox JT, Durrett R, *et al.* (2002) The stepping stone model: New formulas expose old myths. *Annals of Applied Probability*, **12**, 1348–1377.

Currat M, Arenas M, Quilodran C, Excoffier L, Ray N (2019) SPLATCHE3: simulation of serial genetic data under spatially explicit evolutionary scenarios including long-distance dispersal. *Bioinformatics*.

Davis BA, Zanon M, Collins P, *et al.* (2013) The European modern pollen database (EMPD) project. *Vegetation history and archaeobotany*, **22**, 521–530.

De Kort H, Vandepitte K, Bruun HH, Closset-Kopp D, Honnay O, Mergeay J (2014) Landscape genomics and a common garden trial reveal adaptive differentiation to temperature across Europe in the tree species *Alnus glutinosa*. *Molecular Ecology*, **23**, 4709–4721.

De Mita S, Thuillet AC, Gay L, Ahmadi N, Manel S, Ronfort J, Vigouroux Y (2013) Detecting selection along environmental gradients: Analysis of eight methods and their effectiveness for outbreeding and selfing populations. *Molecular Ecology*, **22**, 1383–1399.

Dellicour S, Kastally C, Hardy OJ, Mardulyn P (2014) Comparing phylogeographic hypotheses by simulating dna sequences under a spatially explicit model of coalescence. *Molecular Biology and Evolution*, **31**, 3359–3372.

Drummond AJ, Rambaut A, Shapiro B, Pybus OG (2005) Bayesian coalescent inference of past population dynamics from molecular sequences. *Molecular Biology and Evolution*, **22**, 1185–1192.

Duforet-Frebourg N, Blum MG (2014) Nonstationary patterns of isolation-by-distance: inferring measures of local genetic differentiation with Bayesian kriging. *Evolution*, **68**, 1110–1123.

Elith J, Leathwick JR (2009) Species distribution models: ecological explanation and prediction across space and time. *Annual review of ecology, evolution, and systematics*, **40**, 677–697.

Ellegren H, Galtier N (2016) Determinants of genetic diversity. *Nature Reviews Genetics*, **17**, 422.

Excoffier L, Dupanloup I, Huerta-Sánchez E, Sousa VC, Foll M (2013) Robust demographic inference from genomic and SNP data. *PLoS Genetics*, **9**, e1003905.

Excoffier L, Foll M, Petit RJ (2009) Genetic consequences of range expansions. *Annual Review of Ecology, Evolution, and Systematics*, **40**, 481–501.

Felsenstein J (1976) The theoretical population genetics of variable selection and migration. *Annual Review of Genetics*, **10**, 253–280.

Felsenstein J (1992) Estimating effective population size from samples of sequences: {I}nefficiency of pairwise and segregation sites as compared to phylogenetic estimates. *Genetical Research*, **56**, 139–147.

Forester BR, Jones MR, Joost S, Landguth EL, Lasky JR (2016) Detecting spatial genetic signatures of local adaptation in heterogeneous landscapes. *Molecular Ecology*, **25**, 104–120.

Gavin DG, Fitzpatrick MC, Gugger PF, *et al.* (2014) Climate refugia: joint inference from fossil records, species distribution models and phylogeography. *New Phytologist*, **204**, 37–54.

González-Serna MJ, Cordero PJ, Ortego J (2019) Spatiotemporally explicit demographic modelling supports a joint effect of historical barriers to dispersal and contemporary landscape composition on structuring genomic variation in a red-listed grasshopper. *Molecular ecology*, **28**, 2155–2172.

Guillaume F, Rougemont J (2006) Nemo: an evolutionary and population genetics programming framework. *Bioinformatics*, **22**, 2556–2557.

Guillot G, Estoup A, Mortier F, Cosson JF (2005) A spatial statistical model for landscape genetics. *Genetics*, **170**, 1261–1280.

Haller BC, Messer PW (2019) SLiM 3: Forward genetic simulations beyond the Wright–Fisher model. *Molecular biology and evolution*, **36**, 632–637.

Hanski I, Gilpin M (1991) Metapopulation dynamics: brief history and conceptual domain. *Biological journal of the Linnean Society*, **42**, 3–16.

Hartig F, Dyke J, Hickler T, Higgins SI, O'Hara RB, Scheiter S, Huth A (2012) Connecting dynamic vegetation models to data–an inverse perspective. *Journal of Biogeography*, **39**, 2240–2252.

He Q, Edwards DL, Knowles LL (2013) Integrative testing of how environments from the past to the present shape genetic structure across landscapes. *Evolution*, **67**, 3386–3402.

Hey J, Nielsen R (2007) Integration within the Felsenstein equation for improved Markov chain Monte Carlo methods in population genetics. *Proceedings of the National Academy of Sciences*, **104**, 2785–2790.

Hickerson MJ, Stahl E, Takebayashi N (2007) msBayes: pipeline for testing comparative phylogeographic histories using hierarchical approximate Bayesian computation. *BMC Bioinformatics*, **8**, 268. doi:10.1186/1471-2105-8-268.

Hudson RR, *et al.* (1990) Gene genealogies and the coalescent process. *Oxford surveys in evolutionary biology*, **7**, 44.

Karger DN, Nobis MP, Normand S, Graham CH, Zimmermann NE (2021) Chelsa-trace21k v1. 0. downscaled transient temperature and precipitation data since the last glacial maximum. *Climate of the Past Discussions*, pp. 1–27.

Kaufman D, McKay N, Routson C, *et al.* (2020) A global database of Holocene paleotemperature records. *Scientific data*, **7**, 1–34.

Kelleher J, Etheridge A, Barton NH (2014) Coalescent simulation in continuous space: Algorithms for large neighbourhood size. *Theoretical Population Biology*, **95**, 13–23.

Kelleher J, Etheridge AM, McVean G (2016) Efficient coalescent simulation and genealogical analysis for large sample sizes. *PLoS Computational Biology*, **12**, e1004842.

Kimura M (1953) "Stepping-Stone" model of population. *Annu. Rep. Natl. Inst. Genet*, **3**, 62–63.

Kimura M, Maruyama T (1971) Pattern of neutral polymorphism in a geographically structured population. *Genetics Research*, **18**, 125–131.

Kimura M, Weiss GH (1964) The stepping stone model of population structure and the decrease of genetic correlation with distance. *Genetics*, **49**, 561.

Landguth EL, Cushman S (2010) CDPOP: a spatially explicit cost distance population genetics program. *Molecular ecology resources*, **10**, 156–161.

Leblois R, Rousset F, Tikel D, Moritz C, Estoup A (2000) Absence of evidence for isolation by distance in an expanding cane toad (bufo marinus) population: an individual-based analysis of microsatellite genotypes. *Molecular ecology*, **9**, 1905–1909.

Liepelt S, Cheddadi R, de Beaulieu JL, *et al.* (2009) Postglacial range expansion and its genetic imprints in *Abies alba* (Mill.) - A synthesis from palaeobotanic and genetic data. *Review of Palaeobotany and Palynology*, **153**, 139–149.

Lima-Rezende CA, Rocha AV, Júnior AFC, Martins ÉdS, Vasconcelos V, Caparroz R (2019) Late Pleistocene climatic changes promoted demographic expansion and population reconnection of a Neotropical savanna-adapted bird, *Neothraupis fasciata* (Aves: *Thraupidae*). *PloS one*, **14**, e0212876.

Lima-Ribeiro MS, Varela S, González-Hernández J, de Oliveira G, Diniz-Filho JAF, Terribile LC

(2015) EcoClimate: a database of climate data from multiple models for past, present, and future for macroecologists and biogeographers. *Biodiversity Informatics*, **10**.

Lotterhos KE, Whitlock MC (2014) Evaluation of demographic history and neutral parameterization on the performance of F_{ST} outlier tests. *Molecular Ecology*, **23**, 2178–2192.

Malécot G (1948) *Mathématiques de l'hérédité*. Masson et Cie, Paris.

Malécot G (1955) Remarks on decrease of relationship with distance, following paper by M. Kimura. *Cold Spring Harbor Symposium Quantitative Biololgy*, **20**, 52–53.

Malécot G (1975) Heterozygosity and relationship in regularly subdivided populations. *Theoretical Population Biology*, **8**, 212–241.

Manel S, Schwartz MK, Luikart G, Taberlet P (2003) Landscape genetics: combining landscape ecology and population genetics. *Trends in Ecology & Evolution*, **18**, 189–197.

Maruyama T (1971) An invariant property of a structured population. *Genetical Research*, **18**, 81–84.

Maruyama T (1977) Maruyama lecture notes in biomathematics. 17. Stochastic problems in population genetics.

Meirmans PG (2012) The trouble with isolation by distance. *Molecular Ecology*, **21**, 2839–2846.

Ortego J, Knowles LL (2020) Incorporating interspecific interactions into phylogeographic models: A case study with Californian oaks. *Molecular Ecology*, **29**, 4510–4524.

Pereira HM, Leadley PW, Proença V, *et al.* (2010) Scenarios for global biodiversity in the 21^{st} century. *Science*, **330**, 1496–1501.

Peters KJ, Saltré F, Friedrich T, *et al.* (2019) FosSahul 2.0, an updated database for the Late Quaternary fossil records of Sahul. *Scientific data*, **6**, 1–7.

Quilodrán CS, Nussberger B, Montoya-Burgos JI, Currat M (2019) Hybridization and introgression during density-dependent range expansion: European wildcats as a case study. *Evolution*, **73**, 750–761.

Ralph P, Thornton K, Kelleher J (2020) Efficiently summarizing relationships in large samples: A general duality between statistics of genealogies and genomes. *Genetics*, **215**, 779–797.

Ruosch M, Spahni R, Joos F, Henne PD, Van der Knaap WO, Tinner W (2016) Past and future evolution of *Abies alba* forests in Europe–comparison of a dynamic vegetation model with palaeo data and observations. *Global Change Biology*, **22**, 727–740.

Sexton JP, McIntyre PJ, Angert AL, Rice KJ (2009) Evolution and ecology of species range limits. *Annual Review of Ecology, Evolution, and Systematics*, **40**, 415–436.

Sitch S, Smith B, Prentice IC, *et al.* (2003) Evaluation of ecosystem dynamics, plant geography and terrestrial carbon cycling in the LPJ dynamic global vegetation model. *Global Change Biology*, **9**, 161–185.

Slatkin M (1985) Gene flow in natural populations. *Annual Review of Ecology and Systematics*, **16**, 393–430.

Slatkin M (1991) Inbreeding coefficients and coalescence times. *Genetics Research*, **58**, 167–175.

Slatkin M (1993) Isolation by distance in equilibrium and non-equilibrium populations. *Evolution*, **47**, 264–279.

Smouse PE, Peakall R, Gonzales E (2008) A heterogeneity test for fine-scale genetic structure. *Molecular Ecology*, **17**, 3389–3400.

Sokal RR, Wartenberg DE (1983) A test of spatial autocorrelation analysis using an isolation-by-distance model. *Genetics*, **105**, 219–237.

Strobeck C (1987) Average number of nucleotide differences in a sample from a single subpopulation: a test for population subdivision. *Genetics*, **117**, 149–153.

Svenning JC, Fløjgaard C, Marske KA, Nógues-Bravo D, Normand S (2011) Applications of species distribution modeling to paleobiology. *Quaternary Science Reviews*, **30**, 2930–2947.

Tallavaara M, Luoto M, Korhonen N, Järvinen H, Seppä H (2015) Human population dynamics in Europe over the Last Glacial Maximum. *Proceedings of the National Academy of Sciences*, **112**, 8232–8237.

Tinner W, Colombaroli D, Heiri O, *et al.* (2013) The past ecology of *Abies alba* provides new perspectives on future responses of silver fir forests to global warming. *Ecological Monographs*, **83**, 419–439.

Wakeley J (1998) Segregating sites in Wright's island model. *Theoretical Population Biology*, **53**, 166–174.

Wakeley J (1999) Nonequilibrium migration in human history. *Genetics*, **153**, 1863–1871.

Wang J, Whitlock MC (2003) Estimating effective population size and migration rates from genetic samples over space and time. *Genetics*, **163**, 429–446.

Wang S, Xu X, Shrestha N, Zimmermann NE, Tang Z, Wang Z (2017) Response of spatial vegetation distribution in China to climate changes since the Last Glacial Maximum (LGM). *PloS one*, **12**, e0175742.

Waples RS, Do C, Chopelet J (2011) Calculating n_e and n_e/n in age-structured populations: a hybrid Felsenstein-Hill approach. *Ecology*, **92**, 1513–1522.

706 Whitlock MC, McCauley DE (1999) Indirect measures of gene flow and migration: $F_{ST} \neq 1/(4nm$
707 + 1). *Heredity*, **82**, 117–125.

708 Wright S (1943) Isolation by distance. *Genetics*, **28**, 114.

709 Ziegenhagen B, Fady B, Kuhlenkamp V, Liepelt S (2005) Differentiating groups of abies species
710 with a simple molecular marker. *Silvae Genetica*, **54**, 123–126.

Table 1: Symbols and terms and their definitions.

Symbol	Term	Definition
d	deme	panmictic population in a single grid cell
	map	grid with a defined distribution of deme sizes
L	grid size	number of rows (columns) in a square grid
N	deme size	number of individuals in a deme
N_b	neighbourhood size	size of a focal deme and its four neighbours
T	number of time points	number of time points with the defined demographic history
gt	generation time	the interval between the birth of an individual and the birth of its offspring
dt	time step	time between two defined time points, in years
m	migration rate	fraction of population moving from the ancestral cell to a neighbouring cell
T_W	within-deme coalescence time	coalescence time between two lineages drawn from the same deme
T_B	between-deme coalescence time	coalescence time between two lineages drawn from different demes
T_T	average coalescence time	average coalescence time of any two lineages drawn from the grid

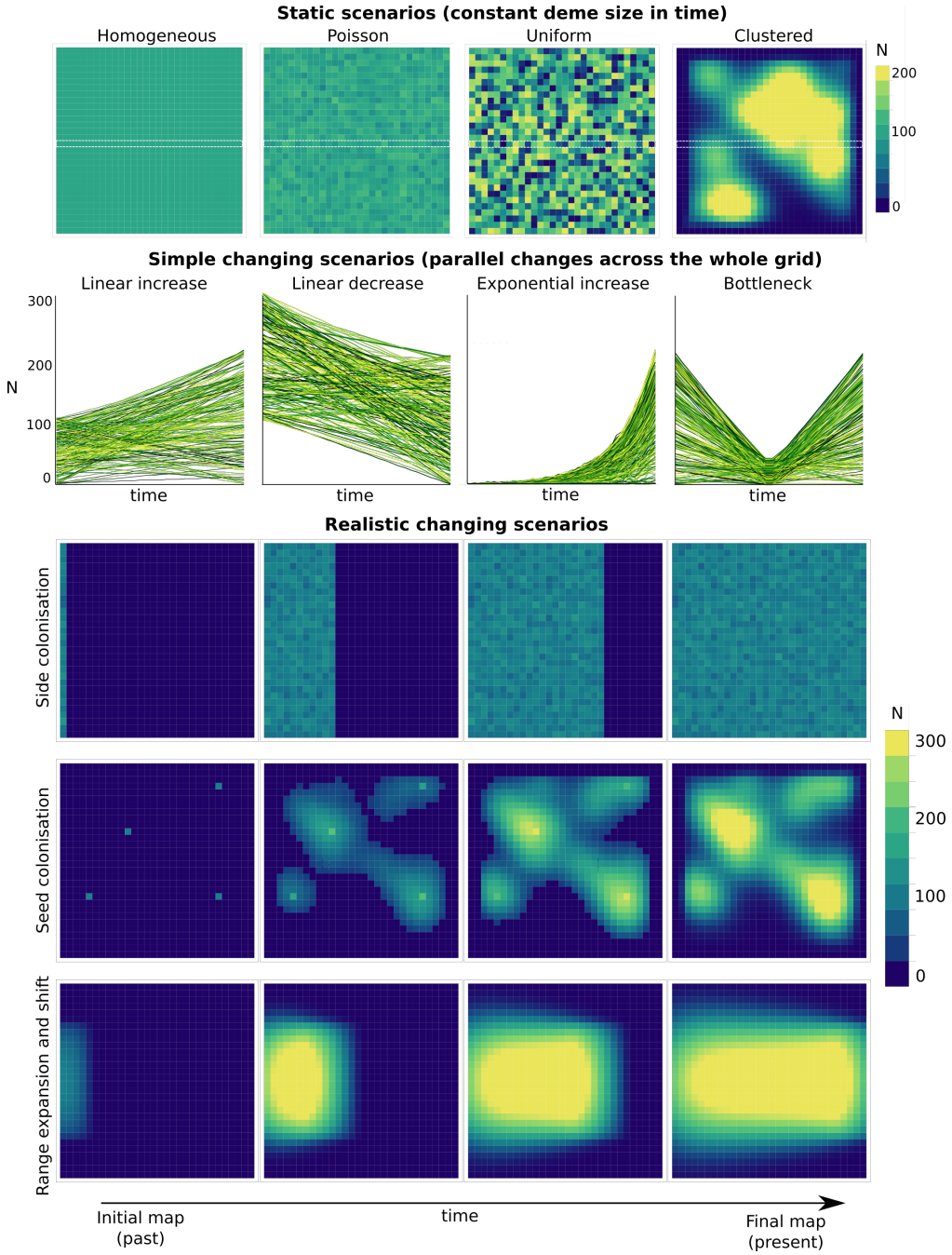

Figure 1: The three different groups of scenarios simulated. **Static scenarios:** demes had a constant size across the spatially explicit phase of the simulations. **Simple changing scenarios:** the size of all demes changed in a correlated manner. In the present time step, all scenarios were identical to the deme sizes drawn from a uniform distribution. **Realistic changing scenarios:** deme sizes changed in space and time to model a colonisation event. The grid size was 30 across all scenarios. To estimate T_W two lineages were sampled in each deme, and to estimate T_B two lineages were sampled from 30 demes in a row in the middle of the grid.

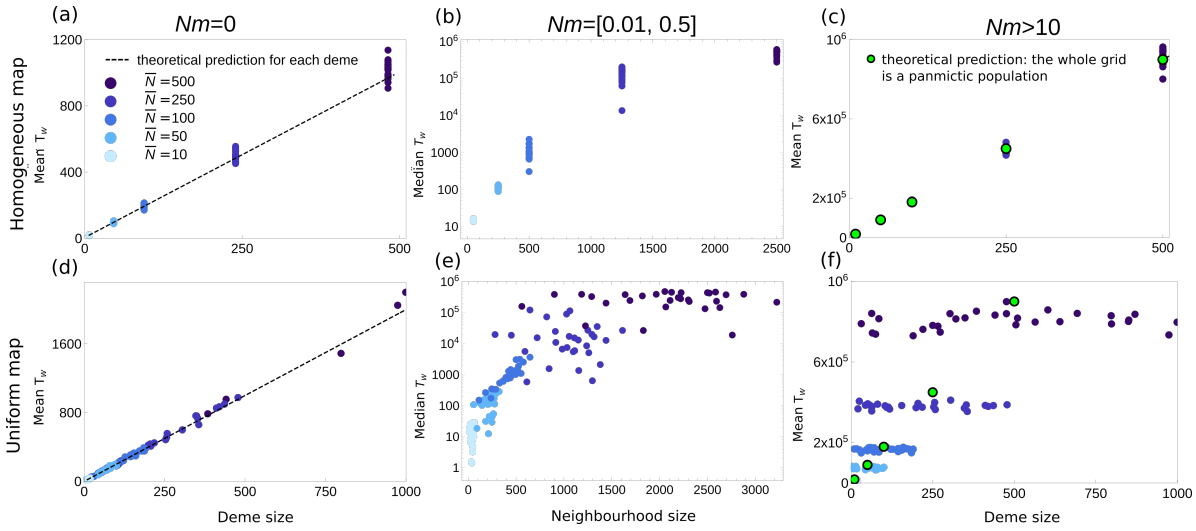

Figure 2: Within-deme coalescence times (T_W) for different ranges of Nm from zero **(a, d)** to $m = 1$ (panmictic grid) **(c, f)** across two maps: homogeneous **(a, b, c)** and uniform **(d, e, f)**. The theoretical predictions are for a Wright-Fisher model with N_i, where i is an index for demes **(a, d)** and for $2L^2\bar{N}$, where L is the grid size and $\bar{N}$ is the average deme size across the grid. There is no theoretical prediction for intermediate Nm **(b, e)** because for those parameter ranges the median T_W is shown. Each parameter combination (N and m) is represented by 30 dots showing T_W for individual demes.

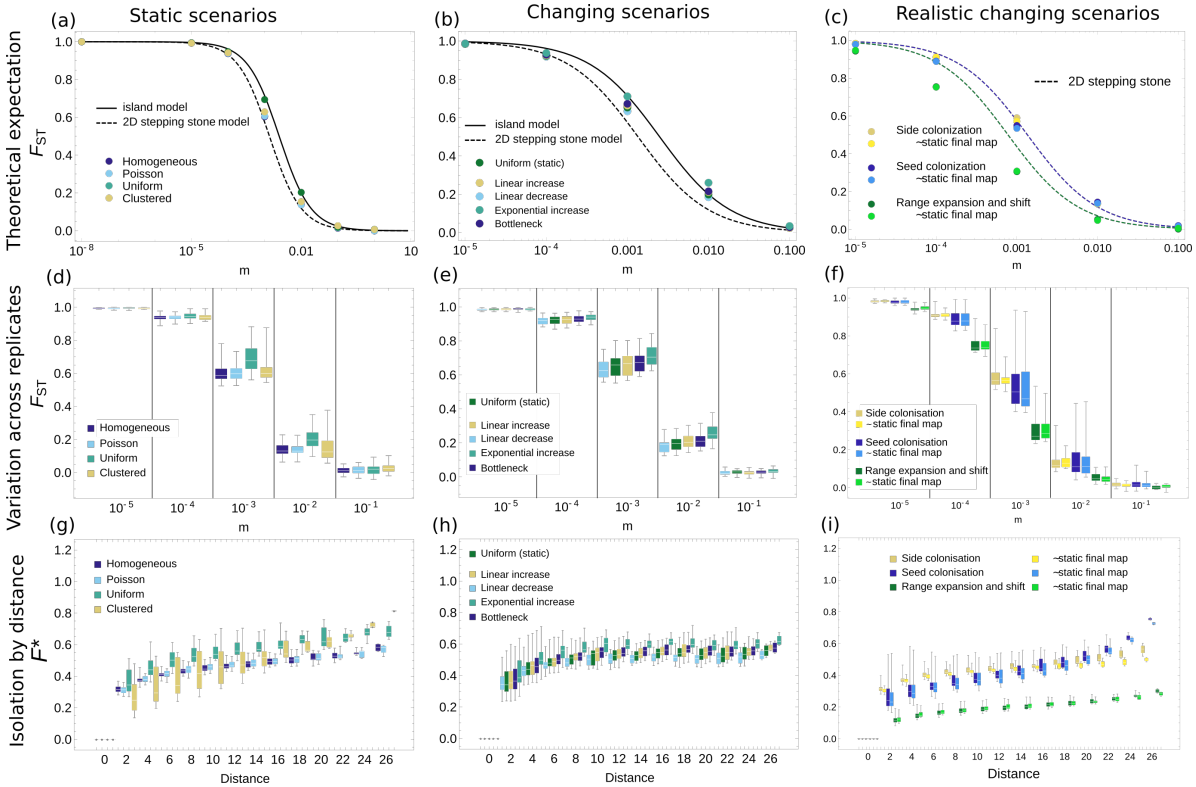

Figure 3: Comparison of F_{ST} from different scenarios with theoretical predictions of the island model and the 2D stepping stone model **(a, b, c)**. Variation in F_{ST} across 1 000 replicate simulations of the same map **(d, e, f)**. Isolation-by-distance patterns characterised as F^* against distance for different scenarios **(g, h, i)**. Simulation parameters: $L = 30$, $T = 30$, $dt = 50000$, $gt = 25$.

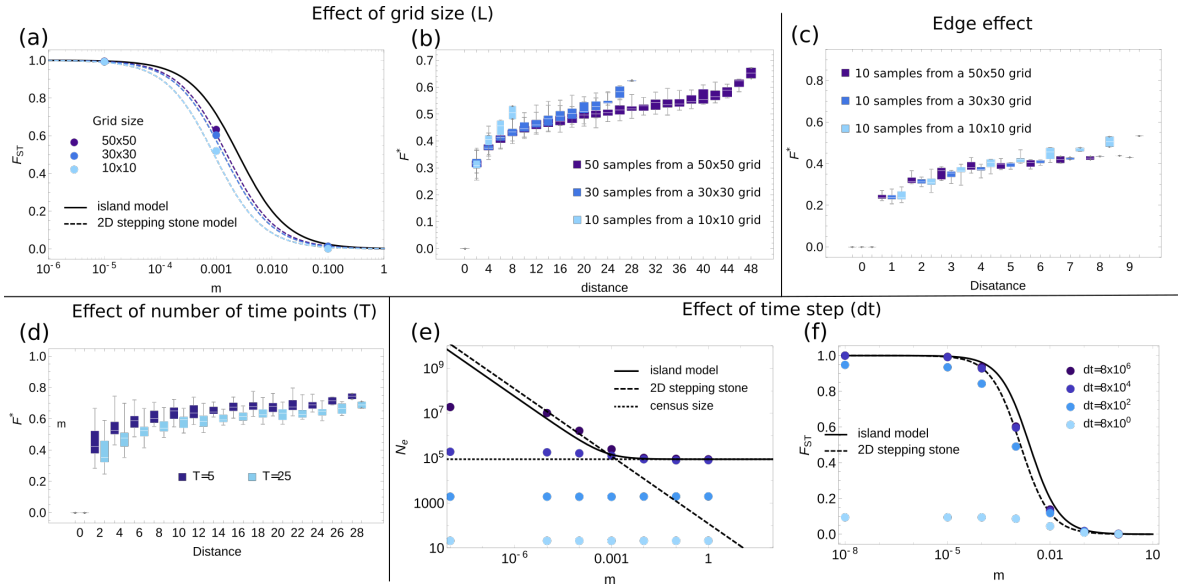

Figure 4: Sensitivity of F_{ST} and F^* to L **(a, b)**, T **(d)**, and N_e (estimated as $T_T/2$, where T_T is the average coalescence time) and F_{ST} to dt **(e, f)** using a homogeneous map, $\overline{N} = 100$, and $m = 10^3$. Unless otherwise specified, $dt = 2 \times 10^8$, $gt = 25$, and $T = 5$. The edge effect **(c)** was explored using inner demes sampled along a line in the middle of the grid.

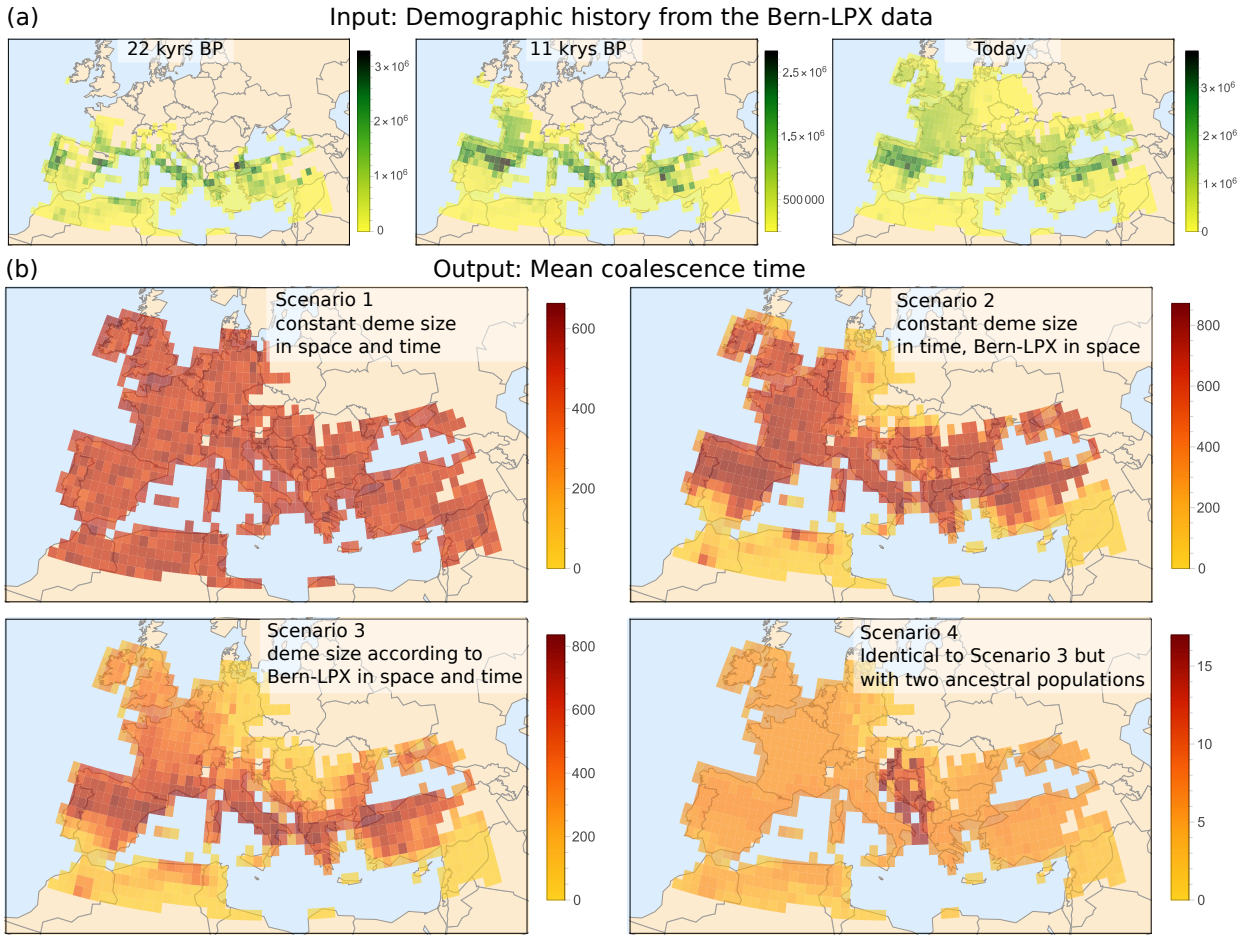

Figure 5: Real-world example: range expansion of silver fir (*Abies alba* Mill.) since the Last Glacial Maximum (LGM, 22 kyrs BP). **(a)** Raw input data for *gridCoal*: the demographic history from the global dynamic vegetation model LPX-Bern. Three time points are shown out of the 220: the LGM, the beginning of the Holocene, and today. **(b)** Mean coalescence time from the simulated scenarios with increasing complexity in terms of spatio-temporal variation in deme size from the top left to the bottom right panel. Note that the colour scale differs between maps.

Supplementary figures

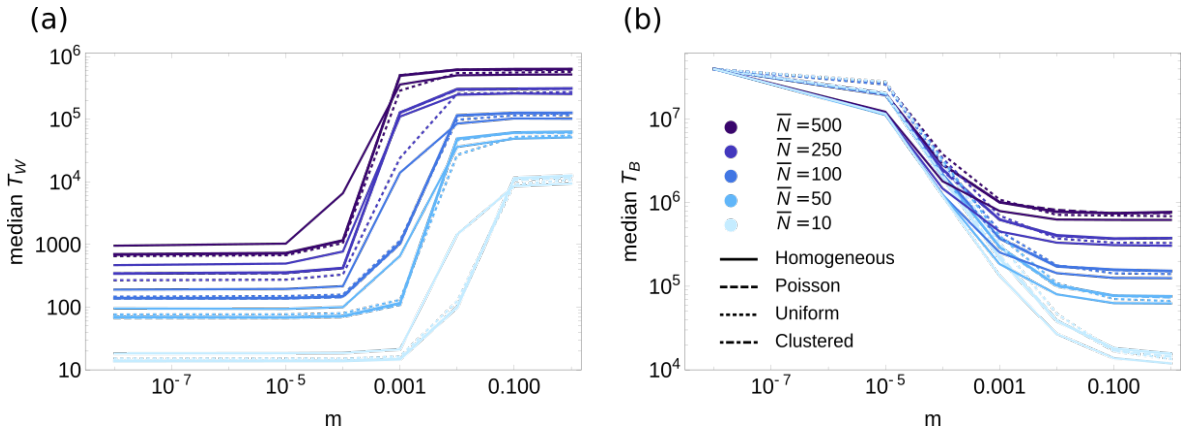

Figure S1: Median coalescence time of two lineages from the same deme T_W **(a)** and from different demes T_B **(b)**. Different line types represent different maps (see Fig. 1 for details).

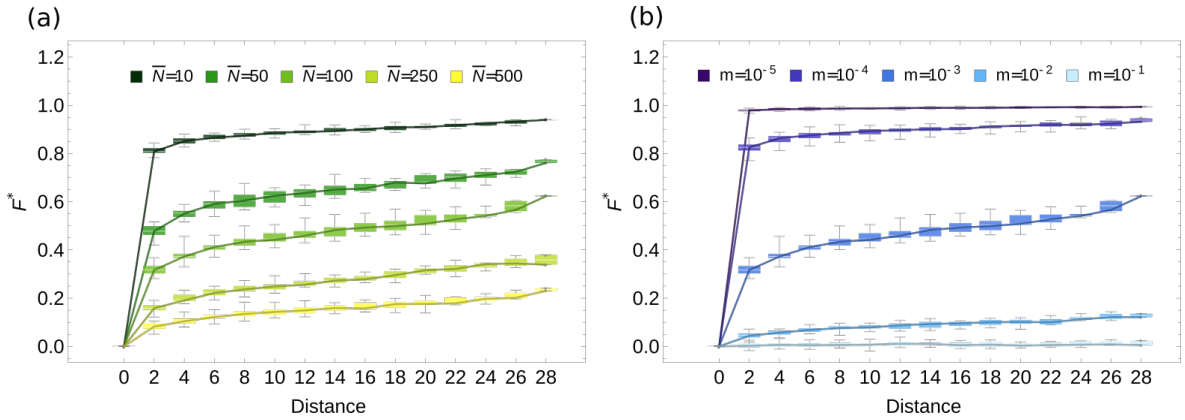

Figure S2: Isolation-by-distance patterns for different average deme sizes, $\bar{N}$ **(a)**, and migration rates, m **(b)**.

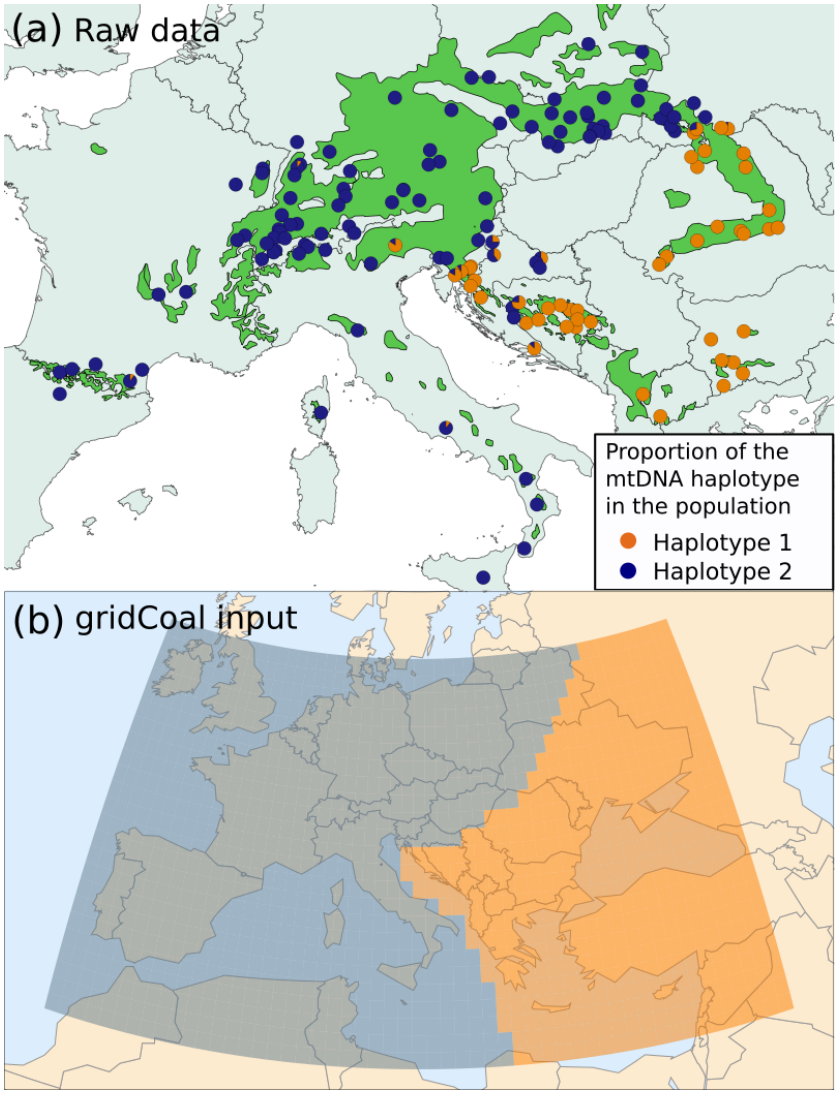

Figure S3: (a) The distribution of silver fir (*Abies alba* Mill.) mtDNA haplotypes in present day samples following (Liepelt *et al.*, 2009) (pie charts) and the distribution of silver fir (in green) from EUFORGEN (`http:\\www.euforgen.org`). **(b)** mtDNA data used to assign each grid cell to one of the two ancestral populations in Scenario 4.

A *gridCoal* description and user manual

A.1 Input files and parameters

In order to run the simulations, it is necessary to define the following input files and parameters.

Demographic history input files [required]: The demographic history of the collection of demes distributed on a grid is represented by a matrix of size $T \times n$, where T is the number of time points at which one wishes to define the population sizes and n is the number of grid cells. The matrix contains the population sizes of the grid cells at given time points. Each row is the flattened two dimensional grid, indexed from 0 to $n-1$, defining the sizes of the subpopulations. The first line is the oldest time point. In *msprime*, a population is not allowed to have size 0. In our case, however, we do not want to exclude the possibility that populations become extinct and the demes are subsequently recolonised, even repeatedly. We therefore set populations with size 0 as 10^{-10}. This is done automatically – before the simulations start, the program replaces any 0 in the input data with 10^{-10}.

Example: demographic history with three data points

1	2	0	4	2	3	4	5	3	4	5	5	4	5	6	7
1	1	1	1	2	2	2	2	3	0	0	3	4	4	4	4
1	2	3	4	2	3	4	5	3	4	5	0	4	5	6	7

Enter as: `-pop InputData.txt` or `--pop_sizes InputData.txt`

Row number [required]: This number, together with the demographic history file, defines the shape of the spatial map. It must be an integer. Additionally, the size of the grid (number of all cells – row length of the demographic history input file) must be divisible by the row number.

Enter as: `-row 5` or `--row_number 5`

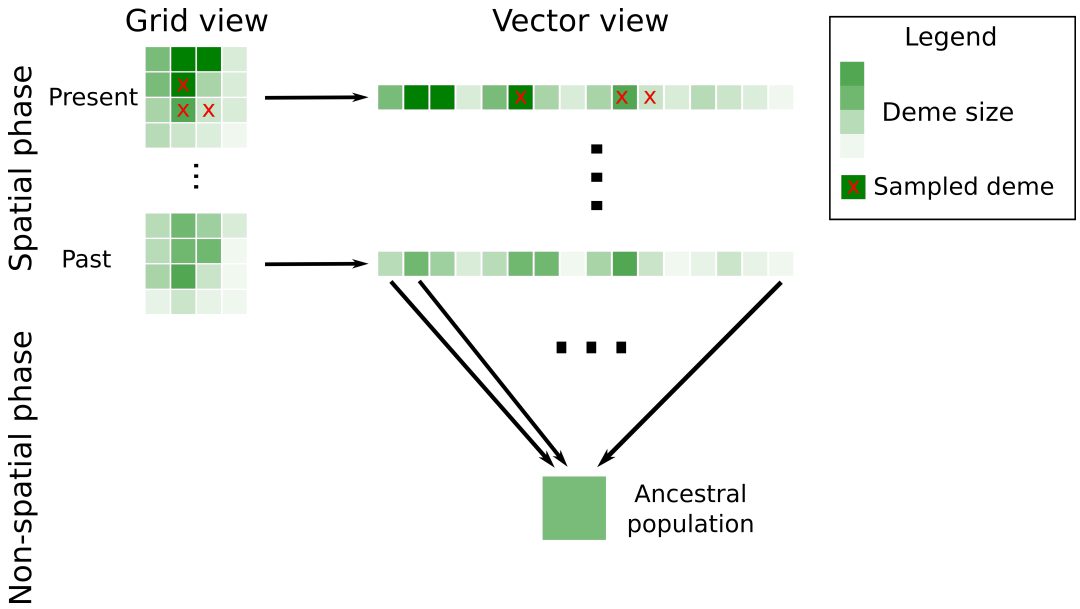

Figure A1: Input data preparation.

List or a fraction of sampled cells [optional]: A list of cells from which the samples are taken is can be suplied. [1]. These cells must not be empty at the final time point (present), but could be empty in the past. For efficiency, two samples are taken from each sampled deme. [2] If only a number (float, < 1) is supplied, random, non-empty cells will be sampled, with the number representing the sampled fraction. If no file is supplied, all samples that are not empty at present are sampled.

Example: SampleList.txt

```
0 1 2 3 4 7 8 33 34 35
```

Enter as: `-sam SampleList.txt` or `--sample_coords SampleList.txt`

[1] Mind the indexing of the sampled cells, which also must start from 0.

[2] It is more efficient to run more replicates with fewer samples than fewer replicates with more samples. In the coalescence process, the waiting time until the next coalescence event happens is exponentially distributed, with its mean proportional to the number of lineages. Thus, in the beginning, several coalescence events happen in quick succession, yet the mean coalescence time of the deme is largely dominated by the amount of time that the last remaining few samples took to coalesce.

Migration matrix A two-dimensional migration matrix capturing backward migration is needed to run the simulation itself; however, as an input file we only need the forward migration matrix, M [3]. We assume that M remains constant in time because it depends on the dispersal ability of the species. The element ($M_{i,j}$) defines the fraction of the lineages in population i that migrates to population j. In order to run coalescence simulations, *gridCoal* calculates a backward migration matrix, BM. BM changes through time, as it depends on the actual population sizes of the neighbouring cells. $BM_{i,j}(t)$ defines the fraction of lineages in population i at time t that have parents in population j and is thus calculated as:

$$BM_{i,j} = \frac{M_{j,i}N_j(t-1)}{N_i(t)} \tag{A1}$$

The fact that the population size changes and migration matrices are not updated at every generation, but at arbitrary time steps, represents a significant gain in computing time in comparison to other tools such as *SPLATCHE 3*.

In the newer version of *gridCoal*, only a migration list is needed, capturing the migration rate from source to target cell.

A migration list indicating the migration rate between two connected cells is used to build a migration matrix, and to calculate backward migration during the simulation. Even if two cells are connected by an edge, if the migration is not specified in the list, it is considered 0. The migration list must be formatted as lines of three values: source cell i (integer), target cell j (integer), and migration rate m_{ij} (positive float between 0 and 1). Note that if migration involves the exchange of migrants, both directions need to be specified.

If a file is not specified but rather a single number m (float) is supplied, a migration matrix is generated in which migration is assumed to occur between adjacent cells symmetrically with rate m.

Example: MigrationList.txt:

[3] The diagonal elements of M must be zero, a requirement for *msprime*.

```
0 1 1.00e-06
0 5 1.00e-06
1 0 1.00e-06
1 2 1.00e-06
1 6 1.00e-06
2 1 1.00e-06
2 3 1.00e-06
2 7 1.00e-06
3 2 1.00e-06
```

Enter as: `-mig MigrationList.txt` or `-mig 0.000001` or `--migration_matrix MigrationList.txt` or `--migration_matrix 0.000001`

Time step and generation time [optional]: The amount of time between two time points, denoted *dt*, is given in arbitrary time units (years, months, days, minutes).

Time is measured in generations in *msprime*, and we therefore need to specify the generation time of the population at hand. We define the generation time, dt, as the time it takes for a species to reach a reproductive age, expressed in the same units as other supplied times. The timing of demographic events (expressed in the same units) is re-calculated by dividing the time point of events specified in demography input files by the generation time of the simulated organism expressed in the same units. Therefore, it is possible to run the simulations for any organism with an arbitrary generation time, from bacterial populations to trees.

By default, generation time is set to 1, and the time between two supplied data points is set at 10.

Enter as: `-dt 100 -gen 25` or `--delta_t 100 --generation_time 25`

Ancestral populations At the point in time beyond which the demography is unknown, all lineages are merged into spatially non-explicit ancestral populations where they follow the standard coalescence process. We assume either a single or multiple panmictic ancestral populations with specified sizes and a very low rate of migration between them (10^{-8}). Furthermore, it is necessary to specify which of the cells originate in each ancestral population.

A list determining the origin of each cell can be supplied as a txt file with n (number of all cells) lines. If no file is supplied, all cells are expected to originate in a single spatially non-explicit population. The size of the ancestral populations can be set, with the default as 1.

Other inputs It is further possible to specify an **output directory**, into which outputs (log file with input parameters, demography debugger, random seed numbers and coalescence times) are saved. The default value is OUTPUT.

Enter as: `--output_dir 7` or `-odir 7`

Print demography file This option can be used to print a detailed demography debugger file, supplied by *msprime*. The replicate number must be set to 1. This makes it possible to simultaneously run many simulations with only one debugger file (identical for all).

Enter as: `-pdeb BOOL` or `--print_debugger BOOL`

Finally, it is possible to set a **random seed number**, which makes it possible to reproduce a given simulation.

Enter as: `--set_seed INT` or `-seed INT`

A.2 Demographic events

All demographic changes, including population size and migration rate changes, need to be defined as a demographic event at a given time point, going backwards in time, and collected to a list, which is used by *msprime* for the coalescence simulation. This is done automatically by *gridCoal* based on the file containing the demographic history.

At each generation, we calculate the backward migration as described above.

Similarly, we update the population sizes, with one additional constraint. If a deme has individuals at a given time point t but was empty in the preceding time point $t - 1$, we need to define the source of those individuals. Specifically, we define a mass migration event from this cell to its 4 neighbouring cells, at rates proportional to their population sizes in the preceding generation. Thinking forward in time, this corresponds to the idea of an empty cell being colonised by its neighbours, at rates proportional to their population sizes.

After a list of demographic events is created, these are supplied to *msprime*, together with the initial conditions. Single repeats are run in each simulation. The coalescence tree is extracted, and the time of coalescence of each pair of samples is saved in matrix format, with sampled cells in rows and columns. The matrix is symmetrical, with the diagonal representing the within-deme coalescence time.

A.3 Output files

Summary of inputs For `REPLICATE = 1`, All the input files are collected and saved into a created `OUTPUT_DIR_NAME` directory as `OUTPUT_DIR_NAME/Output.txt`. The random seed number is saved in the same file.

Print demography debugger If `--print_debugger` is set to `True`, the detailed demographic history – with all changes in population size and migration rate – is produced by *msprime* and printed into the `OUTPUT_DIR_NAME` directory as `OUTPUT_DIR_NAME + 'DemographyDebugger.txt'`. Note that this output file can be very large.

Simulation results The result of the simulation itself is a square matrix of coalescence times of samples from all sampled demes, saved into `OUTPUT_DIR_NAME` directory as

```
838 OUTPUT_DIR_NAME + 'CoalTimes' + REPLICATE + '.txt'
```

B Simulated scenarios

B.1 Static scenarios

In these simulations, all demes had constant sizes across $T = 5$ time points and $dt = 2 \times 10^8$ years (8×10^6 generations, 25 years per generation), on a square grid of size $L = 30$. Different scenarios (maps) were simulated, with increasing spatial variance (see Fig. 1):

- *homogeneous (no spatial variance):* equal-sized demes of size N
- *Poisson (low spatial variance):* deme sizes drawn from a Poisson distribution with mean N
- *uniform (high spatial variance):* deme sizes drawn from a uniform distribution with a range from 0 to $2N$
- *clustered (spatially autocorrelated):* randomly placed seeds grown into clusters, where neighbouring deme sizes were correlated and the average deme size across the whole map was N

Table B1: Summary of parameter values used in the simulations of static populations.

Variable	Symbol	Values
map type		homogeneous, Poisson, uniform, clustered
average deme size size	N	$10, 50, 100, 250, 500$
migration rate	m	0, 10^{-8}, 10^{-5}, 10^{-3}, 10^{-2}, 10^{-1}, 10^{0}

Additionally, to address the effects of grid size and edges due to the finite grid size, we simulated the homogeneous maps on grids with $L \in (10, 30, 50)$ sampling 10, 30 or 50 cells in a line, for only three migration rates, $m \in (10^{-5}, 10^{-3}, 10^{-1})$. To analyse the effect of time resolution and the overall simulation time, we ran simulations on a homogeneous map with deme size $N = 100$ on a square grid of size $L = 30$ with a time step of $dt \in (2 \times 10^2,\ 2 \times 10^4,\ 2 \times 10^6,\ 2 \times 10^8)$ years (generation time was assumed to be 25 years), with migration rates $m \in (0, 10^{-8}, 10^{-5}, 10^{-3}, 10^{-2}, 10^{-1}, 10^{0})$.

B.2 Simple changing scenarios

In these simulations, all demes had a changing but similar demographic history (Fig. 1). Maps were updated at each time point and all scenarios had the same uniform map at the last (most recent) time point $U_{final} = \mathcal{U}(0, 2N)$, where $N = 100$, which ensured a valid comparison across scenarios. Since the deme sizes were changing, we used a finer resolution of $T = 30$ time points and a time step of $dt = 50\,000$ years (2000 generations, 25 years per generation). The following scenarios were simulated:

- *Stable:* there was no change in the average deme size across the map, but we started with a uniform map $U_{startStable} = \mathcal{U}(0, 2N)$ that differed from U_{final}. Therefore, individual deme sizes changed linearly between the initial and final time points.
- *Linear increase:* individual deme sizes changed linearly from a uniform map, with deme sizes drawn from $U_{startLinE} = \mathcal{U}(0, N)$ to U_{final}. Note that while the average deme size increased, some individual demes shrank.
- *Decline:* individual demes changed linearly from a uniform map, with deme sizes drawn from $U_{startDec} = \mathcal{U}(2N, 3N)$ to U_{final}. Note that while the overall population was declining, some demes became larger.
- *Exponential increase:* individual deme sizes increased exponentially from their original sizes, drawn from a uniform distribution $U_{startExpE} = \mathcal{U}(0, 2N)$, to their final sizes U_{final}. Note that while the whole population was expanding, a few individual demes became smaller.
- *Bottleneck:* deme sizes first linearly declined from $U_{startBot} = \mathcal{U}(0, 2N)$ to $U_{midBot} = \mathcal{U}(0, 0.4N)$, then expanded to U_{final}. Note that while the mean deme size changed from N to 0.2N to N again, some individual demes experienced different demographic histories.

Furthermore, we ran a set of simulations where, instead of the uniform map, we used a spatially autocorrelated map (clustered). We ran similar demographic histories, with no change

in time, bottleneck, decline or expansion. We used the same parameters of m, T and step time as used for the homogeneous map.

Table B2: Summary of parameter values used in the simulations of simple demographic histories.

Variable	Symbol	Values
map type		high-variance (uniform)
average deme size	N	100
migration rate	m	10^{-5}, 10^{-4}, 10^{-3}, 10^{-2}, 10^{0}
duration of known demographic history	T	5, 20

B.3 Realistic changing scenarios

These scenarios were inspired by a species range expansion (Fig. 1). Populations colonised the grid from different places so that demes had different demographic histories. As a result, the temporal and spatial autocorrelation were decoupled to some extent. We used the finer resolution of $T = 30$ time points and $dt = 50\ 000$ years (2000 generations, 25 years per generation). The average deme size at the last step was $N = 100$. The following scenarios were simulated:

- *Side colonisation:* demes were colonised from one side of the grid by one column in each of the 30 time points. Once a deme was colonised, its size remained constant.
- *Seed colonisation*: clusters of populations grew from a small number of initially occupied demes or "seeds".
- *Range expansion and shift*: a single expanding population travelled across the grid, while colonising its surroundings. At the first time point, only a kernel of 20×10 demes were occupied. During the following time steps, the kernel demes colonised their neighbours and their size increased by 20% at the next time points.

C Computational run-time of *gridCoal* simulations

We performed 17 500 simulations of *gridCoal* for various parameter sets, to illustrate the dependence of the computational run-time on individual parameters. All simulations were performed on a personal computer with the following specifications:

Operating system:	Mac OS Catalina version 10.15.7
Processor:	2.6 GHz 6-Core Intel Core i7
Memory:	16 GB 2667 MHz DDR4

For each parameter set, 5 batches of 100 simulations (run in series) were run and timed, to account for random effects (e.g. CPU usage by other programs). In the tables below, individual batch measurements are shown and run-time trends are displayed in graphs as a mean and standard deviation of five batches against a changing parameter (in bold). Lines highlighted in green indicate the simulation batch for the same set of parameters. Time was measured using the "time" shell command, with "user" time (measured in seconds) shown in the tables.

Effect of grid size

Output Directory	Seed	Dimensions	Mean population size	Time points	Time step	Generation time	Migration rate	Sampling fraction	Run 1	Run 2	Run 3	Run 4	Run 5	Mean	Standar deviation	Area
GridSize1	1	**5x4**	100	10	200	5	0.1	0.5	1.233	1.207	1.197	1.177	1.208	**1.2044**	0.0203	20
GridSize2	1	**10x8**	100	10	200	5	0.1	0.5	11.108	11.023	10.98	11.099	11.078	**11.0576**	0.0545	80
Baseline	1	**15x12**	100	10	200	5	0.1	0.5	92.962	93.677	93.532	93.095	93.2	**93.2932**	0.3008	180
GridSize4	1	**20x16**	100	10	200	5	0.1	0.5	385.675	381.328	382.483	384.137	381.438	**383.0122**	1.8675	320
GridSize5	1	**25x20**	100	10	200	5	0.1	0.5	1289.598	1280.77	1282.215	1279.916	1281.191	**1282.738**	3.9231	500

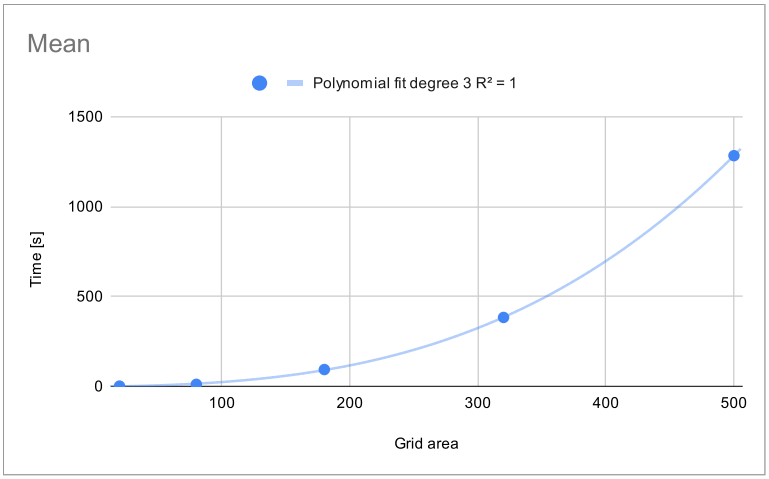

Effect of sampled fraction

Output Directory	Seed	Dimensions	Mean population size	Time points	Time step	Generation time	Migration rate	Sampling fraction	Run 1	Run 2	Run 3	Run 4	Run 5	Mean	Standar deviation
SampledFraction01	1	15x12	100	10	200	5	0.1	**0.1**	22.264	22.241	22.368	22.352	22.225	**22.29**	0.0656
SampledFraction03	1	15x12	100	10	200	5	0.1	**0.3**	53.872	53.88	53.743	53.947	53.933	**53.875**	0.0806
SampledFraction05	1	15x12	100	10	200	5	0.1	**0.5**	86.26	84.539	84.725	84.597	85.83	**85.1902**	0.7978
SampledFraction07	1	15x12	100	10	200	5	0.1	**0.7**	109.865	107.255	107.284	107.682	107.587	**107.9346**	1.0950
SampledFraction1	1	15x12	100	10	200	5	0.1	**1**	151.201	148.181	148.255	150.387	150.401	**149.685**	1.3794

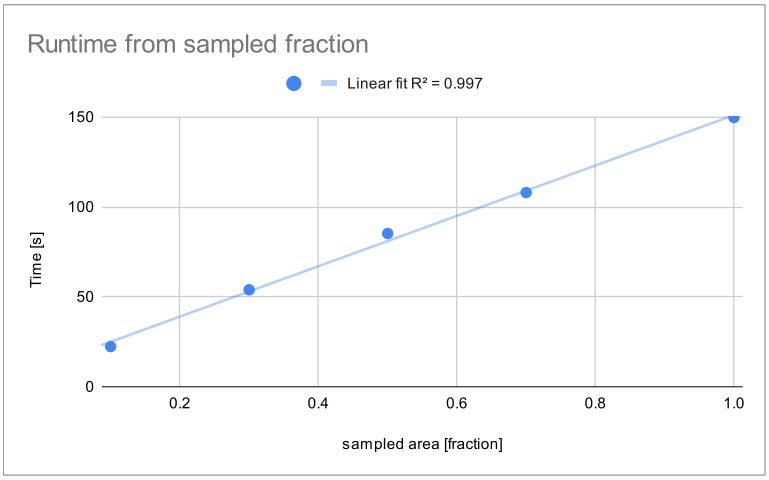

Effect of mean population size

Output Directory	Seed	Dimensions	Mean population size	Time points	Time step	Generation time	Migration rate	Sampling fraction	Run 1	Run 2	Run 3	Run 4	Run 5	Mean	Standar deviation
MeanPopSize10	1	15x12	**10**	10	200	5	0.1	0.5	33.411	33.438	32.921	33.389	33.163	**33.2644**	0.2210
MeanPopSize100	1	15x12	**100**	10	200	5	0.1	0.5	86.761	86.665	86.316	85.975	86.143	**86.372**	0.3355
MeanPopSize500	1	15x12	**500**	10	200	5	0.1	0.5	109.53	108.45	108.626	109.001	108.803	**108.882**	0.4161
MeanPopSize1000	1	15x12	**1000**	10	200	5	0.1	0.5	117.689	117.189	117.565	117.577	117.559	**117.5158**	0.1903
MeanPopSize2000	1	15x12	**2000**	10	200	5	0.1	0.5	127.408	129.057	137.914	138.803	137.408	**134.118**	5.4273

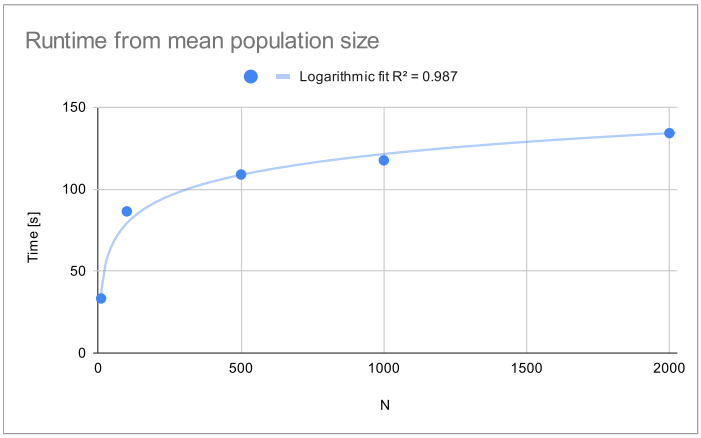

Effect of the number of defined time points

Output Directory	Seed	Dimensions	Mean population size	Time points	Time step	Generation time	Migration rate	Sampling fraction	Run 1	Run 2	Run 3	Run 4	Run 5	Mean	Standar deviation
TimePoints5	1	15x12	100	5	200	5	0.1	0.5	59.327	60.09	57.196	58.492	58.273	**58.6756**	1.0966
TimePoints10	1	15x12	100	10	200	5	0.1	0.5	87.903	84.501	91.794	88.03	88.135	**88.0726**	2.5807
TimePoints20	1	15x12	100	20	200	5	0.1	0.5	128.064	123.701	130.296	129.128	133.872	**129.0122**	3.6874
TimePoints50	1	15x12	100	50	200	5	0.1	0.5	201.55	199.504	199.865	209.857	199.463	**202.0478**	4.4483
TimePoints100	1	15x12	100	100	200	5	0.1	0.5	242.78	246.714	246.313	246.027	246.14	**245.5948**	1.5950

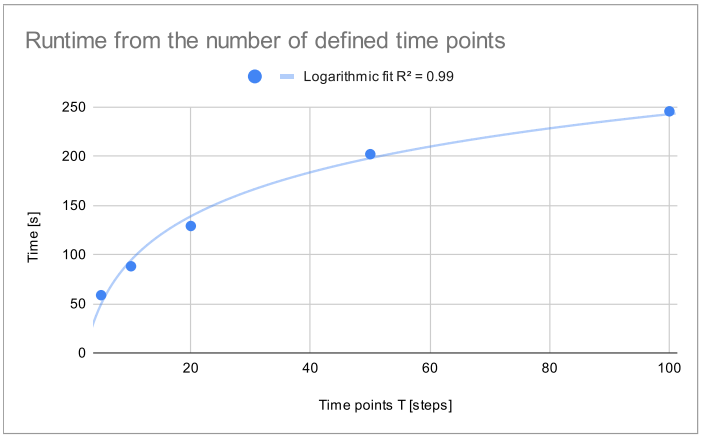

Effect of the generation time

911 Output Directory	Seed	Dimensions	Mean population size	Time points	Time step	Generation time	Migration rate	Sampling fraction	Run 1	Run 2	Run 3	Run 4	Run 5	Mean	Standar deviation
GenTime1	1	15x12	100	10	200	1	0.1	0.5	185.025	178.495	174.344	176.235	176.189	**178.0576**	4.1635
GenTime5	1	15x12	100	10	200	5	0.1	0.5	91.379	89.823	88.743	96.7	89.727	**91.2744**	3.1764
GenTime10	1	15x12	100	10	200	10	0.1	0.5	55.029	54.663	53.67	54.292	57.213	**54.9734**	1.3489
GenTime50	1	15x12	100	10	200	50	0.1	0.5	22.041	23.049	23.138	22.052	21.9	**22.436**	0.6040
GenTime100	1	15x12	100	10	200	100	0.1	0.5	16.679	16.876	16.592	16.422	16.675	**16.6488**	0.1642

912

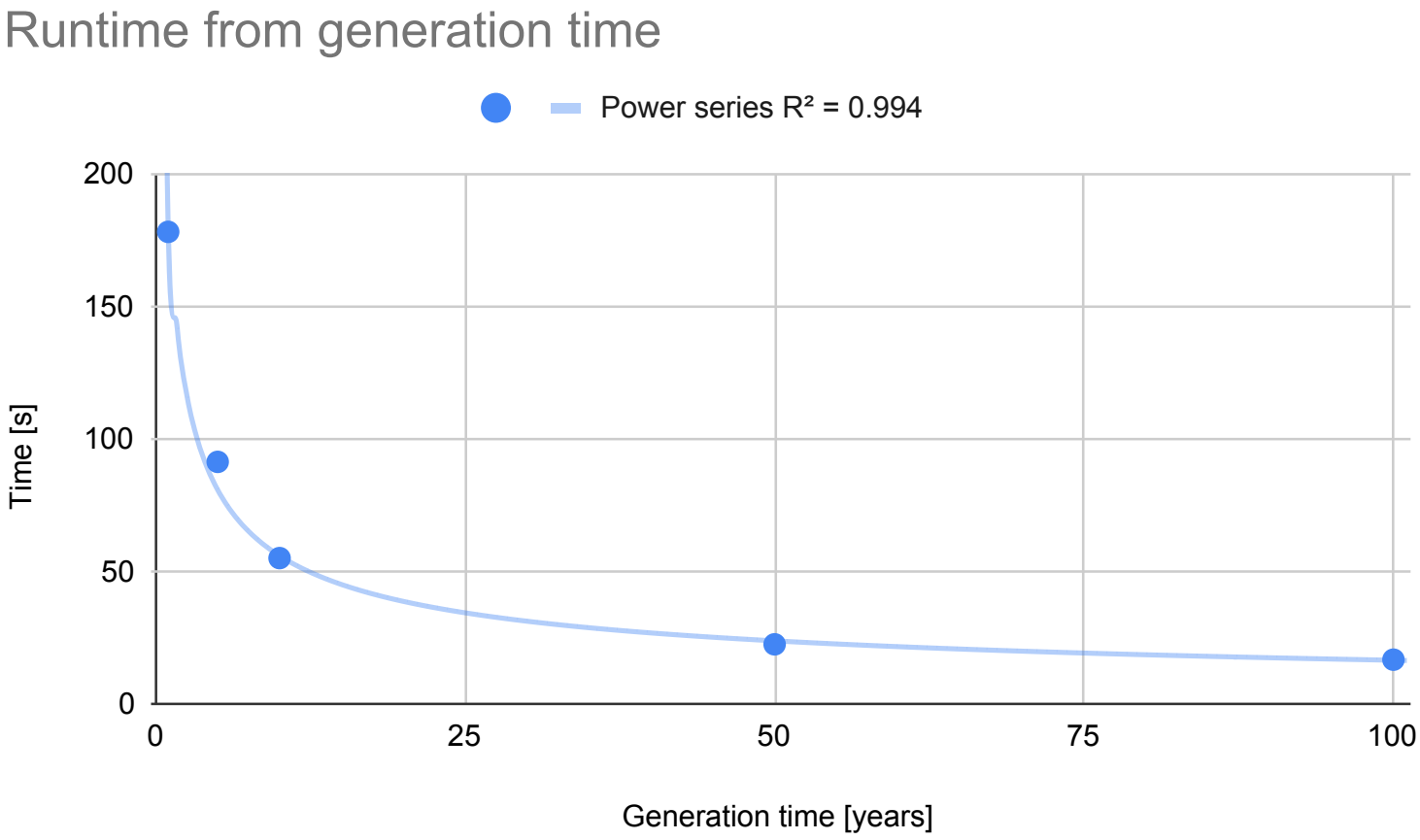
Runtime from generation time
Power series R² = 0.994
200
150
100
50
0
Time [s]
0
25
50
75
100
Generation time [years]